Role of Advection on the Evolution of Near-Surface Temperature and Wind in Urban-Aware Simulations

PALLAV RAY,[a] HAOCHEN TAN,[a] MUKUL TEWARI,[b] JAMES BROWNLEE,[a] R. S. AJAYAMOHAN,[c] AND BRADFORD S. BARRETT[d]

[a] *Meteorology Program, Department of Ocean Engineering and Marine Sciences, Florida Institute of Technology, Melbourne, Florida*
[b] *IBM T. J. Watson Research Center, Yorktown Heights, New York*
[c] *Center for Prototype Climate Modeling, New York University Abu Dhabi, Abu Dhabi, United Arab Emirates*
[d] *U.S. Naval Academy, Annapolis, Maryland*

(Manuscript received 20 March 2020, in final form 11 November 2020)

ABSTRACT: The role of advection of heat and momentum on the evolution of near-surface temperature and wind is evaluated in urban-aware simulations over Houston, Texas, under dry conditions on a light-wind day. Two sets of experiments, each consisting of four simulations using different planetary boundary layer (PBL) schemes, were conducted over 48 h using the default urban scheme (BULK) and the single-layer urban canopy model (SLUCM) available within the Weather Research and Forecasting Model. We focus on understanding and quantifying the role played by temperature and momentum advection, particularly on the windward and leeward sides of the city. Previous studies have largely ignored any quantitative analysis of impacts from the advection of momentum over an urban area. The horizontal advection of temperature was found to be more important in the BULK because of the larger surface temperature gradient caused by warmer surface temperatures over urban areas than in the SLUCM. An analysis of the momentum budget shows that horizontal advection of zonal and meridional momentum plays a prominent role during the period of peak near-surface winds and that this effect is more pronounced in the windward side of the city. The local tendency in peak winds in the leeward side lags that in the windward side by about 1–2 h, similar to the lag found in horizontal momentum advection. The sensitivity of the results to different urban and PBL schemes was explored. The results imply that representation and influence of land-use patterns via sophisticated urban parameterizations generate locally driven winds that best resemble observations.

KEYWORDS: Advection; Moisture/moisture budget; Momentum; Atmosphere–land interaction; Urban meteorology

1. Introduction

To understand the near-surface meteorological conditions in the vicinity of cities, sophisticated urban parameterizations have been developed in recent times (e.g., Kusaka et al. 2001) for a number of models, including the fifth-generation Pennsylvania State University–National Center for Atmospheric Research (NCAR) Mesoscale Model (MM5; Taha 1999; Taha and Bornstein 1999; Dupont et al. 2004; Otte et al. 2004; Liu et al. 2006; Taha 2008a,b), Met Office operational mesoscale model (Best 2005), French MesoNH (Lemonsu and Masson 2002) model, NCAR global climate model (Oleson et al. 2008), and Weather Research and Forecasting (WRF) Model (Tewari et al. 2004; Liu et al. 2006), among others. The development of such urban schemes helps to avoid very high-resolution (order of meters) simulations that would be needed to capture the urban effects in the model adequately. Indeed, near-surface atmospheric structures in urban areas are dependent on the advection of momentum and energy (e.g., Haeger-Eugensson and Holmer 1999; Szymanowski 2005; Heaviside et al. 2015; Bassett et al. 2017). The degree to which the simulated advection of heat and momentum in an urban atmosphere is dependent on the urban parameterizations, planetary boundary layer (PBL) schemes, and their interactions is of great interest.

Advection is an essential component of the budgets of energy and momentum. The effects of temperature advection from the surroundings on the urban weather, and vice versa, have been studied previously by many authors. Recently, Bassett et al. (2017) studied advection of temperature from urban areas to the surrounding rural areas in the United Kingdom. Such urban heat advection (UHA; Lowry 1977) has a profound impact on the PBL as well as surface observations. Bassett et al. (2017) found that UHA from a small urbanized area (~1 km^2) under fair weather conditions (light wind and clear skies) can lead to an increase in nighttime near-surface temperature by 0.6°C at a distance of 0.5 km. Bassett et al. (2016) found an increase in temperature of up to 1.2°C in the downwind areas due to UHA. Belcher et al. (2015), using a street-network model, showed that thermal effects from an urban area could extend 10–15 km downwind because of near-surface temperature advection, in agreement with earlier observational studies (e.g., Dirks 1974; Wong and Dirks 1978).

Although the advection of temperature has been studied extensively, there are far fewer studies on the advection of momentum. Moreover, to the best of our knowledge, no previous studies have been conducted to understand the role of momentum advection on the near-surface winds over an urban area using multiple urban and PBL schemes. Bornstein and Johnson (1977) showed that the urban heat island (UHI) could modify the low-level flow, and more recently, the effect of UHI on winds (e.g., Chen et al. 2011; Lee et al. 2011) and the PBL

Corresponding author: Pallav Ray, pallavkrray@gmail.com; pray@fit.edu

DOI: 10.1175/JAMC-D-20-0068.1

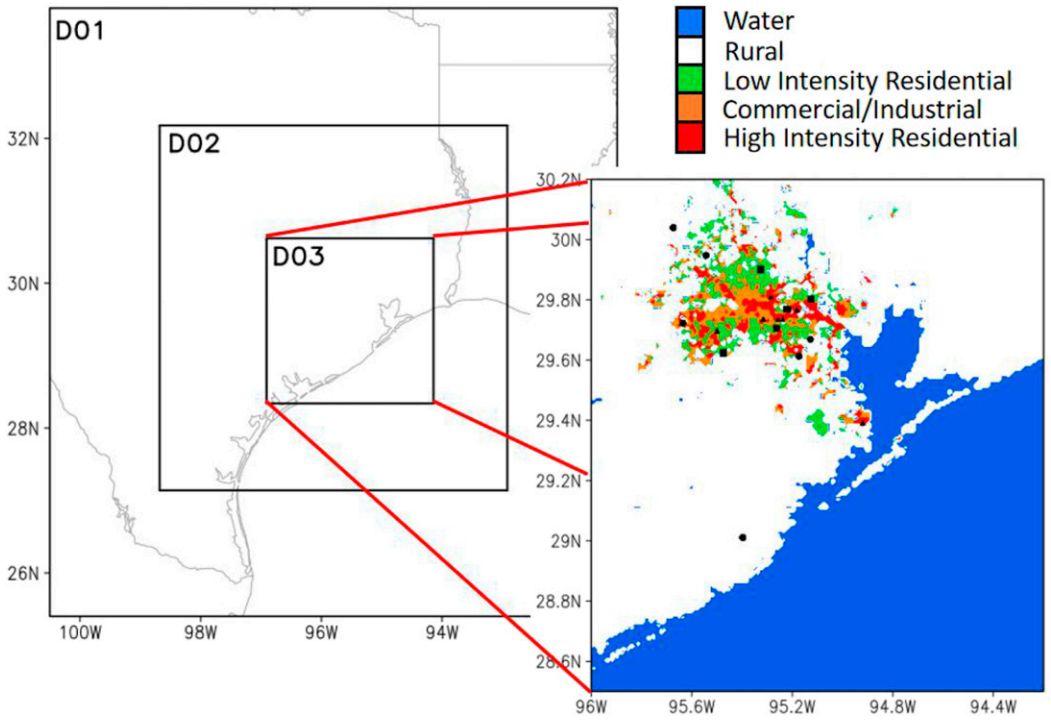

FIG. 1. The configuration of WRF domains with horizontal resolutions of 9 (DO1), 3 (DO2), and 1 (DO3) km. The shading indicates the land-use category of rural (white), LIR (green), HIR (orange), and COI (red) area. Water bodies are marked in blue. The observational stations are marked with circles (rural), squares (LIR) and triangles (COI/HIR). LIR, HIR and COI areas constitute the single urban land category for the BULK simulation.

(e.g., Lee et al. 2011; Zhang et al. 2011) has been demonstrated in several studies. However, the mechanism of such influence, and in particular, the influence from momentum advection on the near-surface winds, has not been quantified. Therefore, in this study, we focus on the role of temperature and momentum advection, and we examine that role in the ensemble mean of simulations performed using different PBL schemes over Houston, Texas. The rest of the paper is organized as follows: Section 2 describes the model, data, and methods, followed by a description of near-surface meteorological conditions in section 3. The role of temperature and momentum advection is explored in section 4. The sensitivity of the results to different urban and PBL schemes is explored briefly in section 5, and discussions and conclusions are given in section 6.

2. Model, data, and methods

The configuration of the model domains using the Advanced Research WRF Model (ARW-WRF; Skamarock et al. 2008), version 3.7, along with the observational stations, is shown in Fig. 1. The inner domains with 3- and 1-km resolutions do not use cumulus parameterization since convection is considered to be resolved at this fine scale. There were 35 vertical sigma levels, of which 8 were located in the lowest 1 km. The model top was set at 50 hPa. The outer domain uses the Kain–Fritsch (KF; Kain 2004) cumulus parameterization since the KF scheme has been found to perform well over urban and coastal areas (Brownlee et al. 2017; Ray et al. 2012; Mittal et al. 2019). The other schemes used in the simulations include the Noah land surface model (Chen and Dudhia 2001), the WSM3 cloud microphysics (Hong et al. 2004), the Dudhia (1989) shortwave scheme, and the RRTM longwave scheme (Mlawer et al. 1997).

All ofthe simulations were integrated from 0000 UTC 24 August to 1800 UTC 26 August 2000 (1800 LST 23 August–1200 LST 26 August 2000). This period was chosen because it was characterized by clear to partly clear skies with little to no organized convection in the vicinity of the Houston area (Nielsen-Gammon 2002). The dominating feature during this time was a well-developed sea-breeze boundary, which formed in the early afternoon of 25 August and moved inland toward Houston in the late afternoon (Nielsen-Gammon 2002; Cheng and Byun 2008). The surface was characterized by light southeasterly winds, which remained until around late evening [1900 central daylight time (CDT)]. This weather pattern helps to avoid complexities generally associated with moist convection. Given the computational expense of each high-resolution simulation over an urban area, simulation over a short period has been a common strategy (e.g., Fan and Sailor 2005; Salamanca et al. 2011; García-Díez et al. 2013; Banks et al. 2016; Huang et al. 2019; Tan et al. 2019). For example, Fan and Sailor (2005) and Salamanca et al. (2011) used two days of simulation, García-Díez et al. (2013) used 42 h of simulation, and Banks et al. (2016) computed for 36 h. The studies that relied on longer simulation typically employed much coarser

TABLE 1. Summary of PBL schemes used in this study.

PBL schemes	Closure type	References	Simulations
Yonsei University (YSU)	1 nonlocal	Hong et al. (2006)	A total of eight simulations
Mellor–Yamada–Janjić (MYJ)	1.5 local	Janjić (1994)	were performed: four using
Mellor–Yamada–Nakanishi–Niño level 2.5 (MYNN2)	1.5 local	Nakanishi and Niino (2006, 2009)	the BULK and four using
Bougeault–Lacarrere (BouLac)	1.5 local	Bougeault and Lacarrere (1989)	the SLUCM urban schemes

horizontal resolution; for example, Gunwani and Mohan (2017) ran a 10-km-resolution simulation over 17 days. On the other hand, results based on short-term simulations like ours may not be truly representative of the model's performance for long-term simulations, and thus need to be treated with caution (García-Díez et al. 2013).

Model output was saved every 10 min to capture the diurnal evolution of the atmospheric structure adequately. The near-surface observations were taken from the 18 Texas Commission on Environmental Quality (TCEQ) stations that provide hourly data. For model-data comparisons, both were hourly averaged for consistency. Of 18 stations, 6 are in a rural category and 12 are in an urban land-use category. Most TCEQ station observations are taken at 11-m height, but a few stations take observations at 4–5-m height. The land-use data were taken from the 2001 National Land Cover Database (NLCD; 30-m resolution). The model initial and boundary conditions were taken from the National Centers for Environmental Prediction (NCEP) final analysis (NCEP_FNL; $1° \times 1°$ and 6 hourly). The wind and temperature from the ERA-Interim reanalysis (Dee et al. 2011; ~80 km) were also used for comparison with the simulations. Further details about the model configurations can be found in Brownlee et al. (2017).

Two sets of urban schemes were tested in conjunction with four different common PBL schemes, leading to a total of eight simulations (Table 1). This combination of schemes was needed because the WRF Model, like other models, yields different near-surface conditions depending on the urban and PBL schemes (e.g., Jiménez et al. 2013; Huang et al. 2019). The first set of simulations used the default urban scheme (BULK; Tewari et al. 2004; Liu et al. 2006), and the second set of simulations used the original single-layer urban canopy model (SLUCM; Kusaka et al. 2001; Kusaka and Kimura 2004; Yang et al. 2014). In the BULK urban scheme, typical urban characteristics (e.g., emissivity, albedo, thermal conductivity) are provided, and the scheme considers the urban areas to have 100% artificial surfaces. The BULK scheme has been used in both research and real-time forecasts (Liu et al. 2006). In the SLUCM urban scheme, a representative urban canopy that includes a mixture of artificial and natural surfaces is considered. For example, urban fraction in the SLUCM in light-intensity residential (LIR), high-intensity residential (HIR), and commercial–industrial (COI) areas is 50%, 90%, and 95%, respectively. Three different urban surfaces (roof, wall, and roads) are recognized. We have used the default parameters in the BULK and the SLUCM schemes since Lee et al. (2011) showed that near-surface conditions over the Houston area are not very sensitive to the choice of urban parameters over Houston.

Of the four PBL schemes (Table 1) tested, the YSU scheme is a first-order nonlocal scheme, and the rest are local schemes with closures higher than order one. Since our numerical experiments were conducted under dry conditions on a light-wind day, we chose three local schemes and one nonlocal scheme. In WRF, PBL schemes mix not only in the PBL, but also handle vertical mixing in the whole column. Although nonlocal schemes typically outperform local schemes in a convective atmosphere (e.g., Hu et al. 2010), local schemes can perform reasonably well during stable conditions (e.g., Cohen et al. 2015). Moreover, some local schemes have been improved with the addition of more prognostic terms to create a well-mixed and deep PBL (Nakanishi and Niino 2009), changes that have allowed them to outperform nonlocal schemes (Coniglio et al. 2013). All four chosen PBL schemes are popular and have been used extensively in other studies (e.g., Xie et al. 2012; Banks et al. 2016). For a detailed survey of these PBL schemes, readers are encouraged to see Cohen et al. (2015).

3. Near-surface conditions

We provide a brief description of the model evaluation for near-surface conditions including the 2-m temperature and 10-m winds. A detailed model validation can be found in Brownlee (2016) and Brownlee et al. (2017).

a. Temperature and winds

Figure 2 shows the 2-m temperature (T2) and 10-m horizontal winds (W10) from the model ensemble mean of BULK and SLUCM simulations and compared with observations. As mentioned earlier, most observation sites take measurements of temperature and winds at 11-m height, while a few stations take measurements at 4–5-m height. We have not applied any corrections for this difference in measurement heights between the model and observations. For brevity, hereinafter, we refer to the two ensemble means as BULK and SLUCM. In BULK, the T2 is warmer than the observation sites in both LIR and COI/HIR land categories. In the rural areas, the simulated T2 is nearly the same in both the BULK and the SLUCM (Fig. 2a). This is expected since the urban schemes do not affect the rural areas directly. The performance of the ensemble mean and the individual PBL schemes (described later in section 5) concerning mean error and the root-mean-squared error (RMSE) is given in Tables 2–4.

For the 10-m winds (Fig. 2, bottom), it is interesting that for all urban configurations, the simulated winds are generally lower than the observations in the morning, but during the early evening and overnight periods, they are higher than the observations. This discrepancy, at least partly, is because

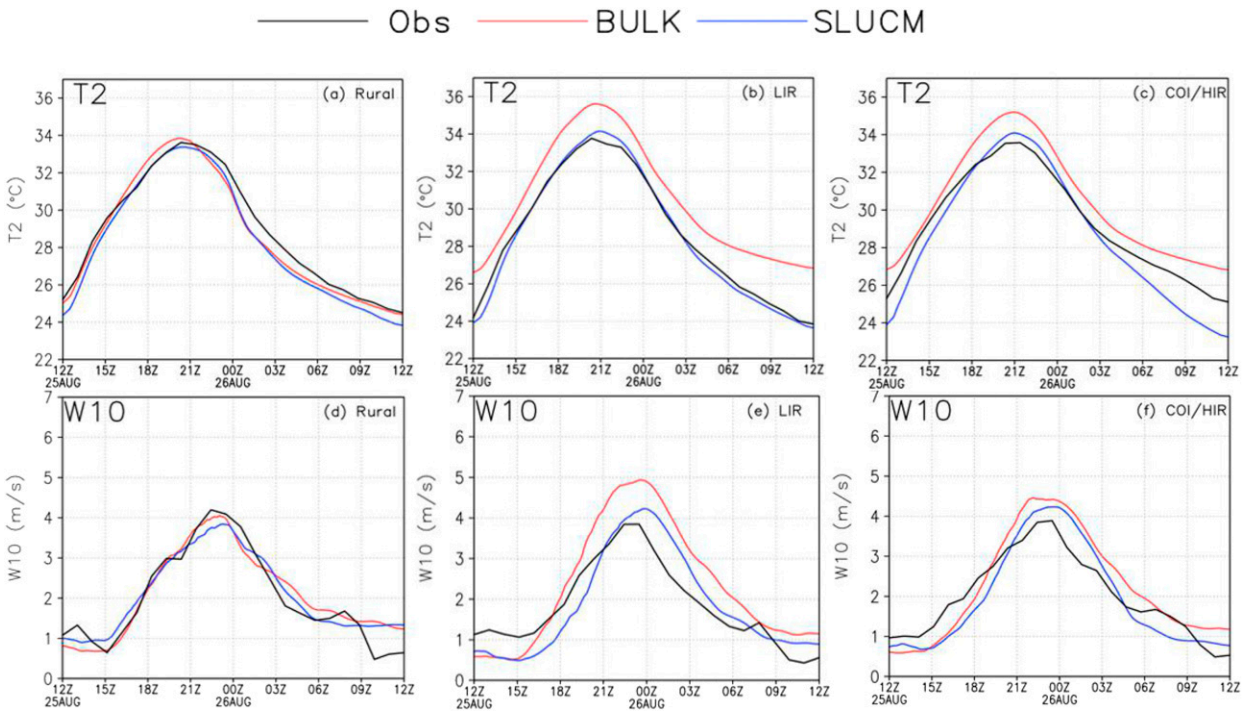

FIG. 2. The (a)–(c) 2-m temperature (T2; °C) and (d)–(f) 10-m wind (W10; m s^{-1}) from the BULK (red), SLUCM (blue), and observations (black) in land categories (left) rural, (center) LIR, and(right) COI/HIR over all observing stations that are marked as black circles (rural), squares (LIR), and triangles (COI/HIR) in Fig. 1. The time is in UTC. The Houston local time is UTC minus 6 h.

the afternoon simulated winds peak later than the observations. As a result of this, there is a phase lag (~1.5 h) between the simulations and the observations. The averaged observed wind speed during the 24-h time-period (1200 UTC 25 August–1200 UTC 26 August) over rural areas (1.99 m s^{-1}) is slightly higher than that in the urban areas (1.91 m s^{-1}). This relationship is not captured by the BULK scheme, where the wind speed is higher over urban areas (2.35 m s^{-1}) than in rural areas (2.10 m s^{-1}). This is because surface sensible heat flux is much higher in the BULK over urban areas (see section 3b), leading to a much vigorous mixing and higher near-surface winds over urban areas than rural areas (e.g., Lee et al. 2011; Brownlee et al. 2017). However, the observed relationship between the rural and urban surface winds is well captured by the SLUCM. For example, the averaged wind speed over rural and urban stations in the SLUCM is 2.09 and 1.87 m s^{-1}, respectively.

Over urban areas, the mean bias and RMSE in T2 and W10 are larger in BULK than in SLUCM (Tables 3 and 4), and both simulations produced stronger winds than the observations. This result is consistent with Shimada et al. (2011), who also

TABLE 2. The RMSE and mean bias of 2-m temperature (°C) and 10-m wind (m s^{-1}) from 1200 UTC (0600 LST) 25 Aug to 1200 UTC (0600 LST) 26 Aug 2000 over rural areas. The best performance in a group (lowest bias and lowest RMSE) is indicated with boldface type. Daytime was from 0600 LST 25 Aug to 1800 LST 25 Aug, and nighttime was from 1800 LST 25 Aug to 0600 LST 26 Aug.

	T2 bias			T2 RMSE			W10 bias			W10 RMSE		
PBL	Total	Day	Night	Total	Day	Night	Total	Day	Night	Total	Day	Night
						BULK						
Ensemble	−0.15	−0.37	**0.06**	0.53	**0.51**	**0.59**	0.21	0.12	0.31	0.49	**0.40**	**0.59**
YSU	−0.24	−0.36	−0.11	**0.44**	0.56	0.65	0.17	−0.02	0.34	0.45	0.42	0.61
MYJ	−0.17	−0.39	**0.06**	0.56	0.80	0.62	0.37	0.35	0.38	0.49	0.45	0.78
MYNN	−0.29	−0.49	−0.07	0.55	0.76	0.67	0.17	**−0.01**	0.33	0.58	0.52	0.74
BouLac	**0.05**	**−0.25**	0.35	0.57	0.73	0.93	**0.12**	0.18	**0.05**	**0.44**	0.41	0.78
						SLUCM						
Ensemble	−0.55	−0.52	−0.59	0.65	**0.46**	0.78	0.20	−0.04	**0.25**	0.42	0.39	0.70
YSU	−0.55	−0.45	−0.54	0.62	0.53	0.85	0.28	−0.03	0.59	0.44	0.42	0.81
MYJ	−0.57	−0.60	−0.43	0.68	0.76	0.73	0.25	**0.01**	0.48	0.41	0.29	0.81
MYNN	−0.72	−0.68	−0.76	0.78	0.76	0.99	0.18	−0.04	0.39	0.46	0.46	**0.67**
BouLac	**−0.34**	**−0.36**	**−0.33**	**0.53**	0.65	**0.56**	**0.12**	−0.10	0.33	**0.35**	**0.28**	**0.67**

TABLE 3. As in Table 2, but for LIR.

PBL	T2 bias			T2 RMSE			W10 bias			W10 RMSE		
	Total	Day	Night	Total	Day	Night	Total	Day	Night	Total	Day	Night
BULK												
Ensemble	1.89	1.69	2.04	1.98	**1.40**	**2.21**	0.69	1.03	0.33	0.98	1.09	**0.48**
YSU	**1.69**	**1.42**	**1.89**	**1.87**	1.47	2.52	**0.46**	**0.52**	0.42	**0.62**	**0.57**	0.62
MYJ	1.87	1.68	1.98	1.94	1.72	2.96	0.87	1.35	0.29	1.19	1.42	0.83
MYNN	1.83	1.61	1.93	1.90	1.63	2.92	0.73	1.11	0.30	1.06	1.18	0.96
BouLac	2.17	2.06	2.30	2.22	2.08	3.33	0.69	1.14	**−0.03**	1.06	1.25	0.83
SLUCM												
Ensemble	−0.06	0.13	−0.24	0.35	0.29	0.68	0.21	0.25	0.18	0.62	0.58	**0.50**
YSU	−0.21	0.15	−0.68	0.49	0.27	0.81	0.47	0.59	0.25	0.72	0.74	0.58
MYJ	**−0.04**	0.06	−0.14	**0.20**	**0.25**	**0.66**	**0.09**	**0.03**	0.15	**0.51**	**0.54**	0.66
MYNN	−0.22	**−0.03**	−0.42	0.36	**0.25**	0.99	0.19	0.17	0.22	0.64	0.67	0.90
BouLac	0.23	0.34	**0.12**	0.34	0.50	0.81	**0.09**	0.19	**−0.05**	0.62	0.57	0.81

found a positive mean bias for the near-surface wind speed. Sarmiento et al. (2017), in their work, presented a comprehensive assessment of the WRF-Urban modeling system for the Indianapolis region and found that the wind speed near the surface exhibited an overestimation in various model configurations. Further discussions on T2 and W10, and their dependence on PBL schemes, are given in section 5.

The horizontal structure of temperature at 2 m and 950 hPa is shown in Fig. 3 (shaded). The warmer near-surface temperature over urban areas in the BULK (Fig. 3b) and SLUCM schemes (Fig. 3c) is not seen in the reanalysis (Fig. 3a). The difference in temperature feeds back to the pressure gradient and thus drives a difference in winds, and these differences in temperature and winds can be seen at 950 hPa (Fig. 3, bottom). In the ERA-Interim (Figs. 3a,d), the wind is predominantly southerly over land and does not show any changes due to the urban areas, a difference that is likely related to its coarse resolution. When the BULK and SLUCM urban parameterizations are used together with a horizontal resolution that is sufficiently fine to resolve urban areas (Figs. 3b,c,e,f), the modulation of winds by the urban areas can be seen clearly over the land as an easterly zonal component.

Since the reanalysis does not capture the urban and rural near-surface temperature differences (Fig. 3a), we analyze the surface skin temperature from the BULK (Fig. 4a) and the SLUCM (Fig. 4b) only. The skin temperature is much higher in the BULK than the SLUCM due to less moisture on the BULK surface. Salamanca et al. (2018) found that bulk urban parameterization overestimates nighttime 2-m temperature compared to the single-layer urban canopy model (UCM) and multilayer UCM in their study of evaluation of WRF-Urban modeling system over a semiarid urban environment. The UHI intensity from the model simulations (Fig. 4c) shows that the peak intensity is also higher in the BULK than the SLUCM, but the overall temporal variation is similar in both simulations with a time-offset of about 3 h. The UHI intensity has likely been overestimated by the BULK, given that BULK simulation overestimated temperature over urban areas and not in rural areas (Figs. 2b,c).

b. *Surface heat flux*

Figure 5 shows the surface latent (Q_{LH}) and sensible (Q_{SH}) heat fluxes as well as net shortwave (Q_{SW}) and net longwave (Q_{LW}) radiation from the BULK and the SLUCM over all land-use types. The Q_{LH} is very small in the city in the BULK ($<5\,W\,m^{-2}$, Fig. 4a) and increases significantly when the SLUCM configuration is implemented (Fig. 5c, Table 5). This difference, when changing from the BULK to the SLUCM

TABLE 4. As in Table 2, but for COI/HIR.

PBL	T2 bias			T2 RMSE			W10 bias			W10 RMSE		
	Total	Day	Night	Total	Day	Night	Total	Day	Night	Total	Day	Night
BULK												
Ensemble	1.16	1.25	1.04	1.24	1.18	1.55	0.42	0.84	**−0.02**	0.77	0.78	0.61
YSU	**0.96**	**1.02**	**0.90**	**1.03**	**1.10**	**1.50**	**0.18**	**0.19**	0.17	**0.41**	**0.31**	**0.58**
MYJ	1.12	1.21	1.02	1.21	1.29	1.78	0.63	0.72	0.54	0.97	0.87	0.63
MYNN	1.09	1.20	0.97	1.17	1.25	1.72	0.43	0.58	0.25	0.83	0.69	0.69
BouLac	1.45	1.49	1.41	1.54	1.55	2.04	0.43	0.86	−0.08	0.87	0.79	0.77
SLUCM												
Ensemble	−0.50	**0.02**	−1.02	0.97	0.61	1.85	**−0.02**	0.15	−0.19	0.55	0.50	**0.41**
YSU	−0.81	−0.3	−1.32	1.25	0.51	1.96	0.25	0.66	**−0.17**	0.55	0.59	0.44
MYJ	−0.55	−0.11	−0.90	0.86	0.47	1.45	−0.08	**0.02**	−0.20	**0.51**	**0.46**	0.62
MYNN	−0.68	−0.03	−1.17	0.97	**0.46**	1.82	−0.09	0.09	−0.27	0.57	**0.46**	0.78
BouLac	**−0.27**	0.21	**−0.74**	**0.79**	0.59	**1.30**	0.42	0.28	0.67	0.57	0.52	0.75

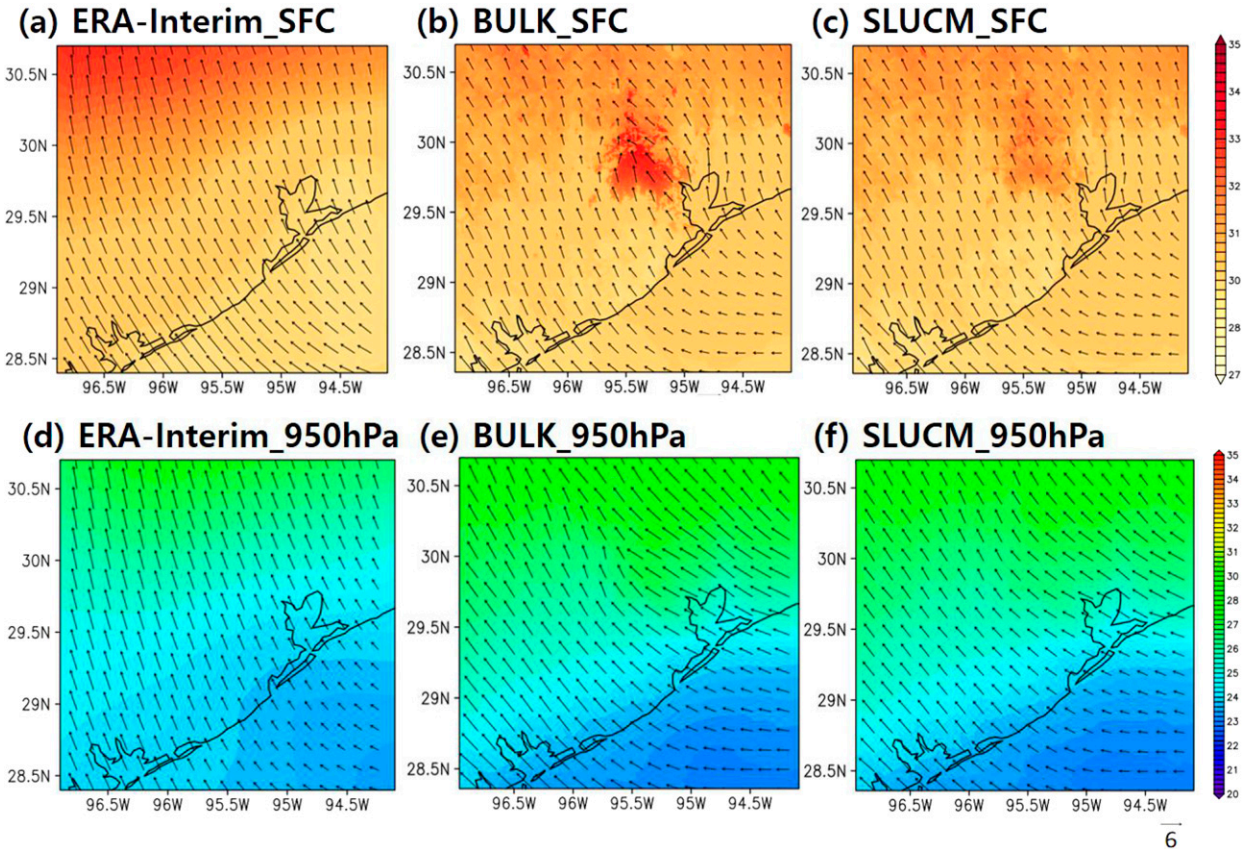

FIG. 3. The temperature (shaded; °C) and horizontal winds (vectors; m s^{-1}) at (top) 2 and 10 m, respectively, and (bottom) the 950-hPa level from the (a),(d) ERA-Interim; (b),(e) BULK; and (c),(f) SLUCM averaged from 1800 UTC 25 Aug to 0600 UTC 26 Aug 2000. All panels use data that are based on 80-km grid-spacing for a consistent comparison, and a reference wind vector is provided below (f).

scheme, arises because the BULK scheme assumes the urban areas to be impervious (Yang et al. 2014), resulting in little to no moisture at the urban surface. As a result, the Q_{LH} is nearly zero over urban areas. In the SLUCM, where a representative urban canopy is used, much higher Q_{LH} is simulated than that in BULK. Sharma et al. (2016) discussed the lower latent heat flux for urban than rural areas in their urban modeling study over the Chicago area. They found an increase in the latent heat flux using the mosaic approach in urban areas due to a better representation of nonurban classes. On the other hand, the Q_{SH} is much larger in BULK (Fig. 5b) compared to the SLUCM (Fig. 5d). For example, the peak Q_{SH} is over 400 W m^{-2} in the BULK (Fig. 5b) but decreases to less than 300 W m^{-2} in the SLUCM (Fig. 5d).

For Q_{SW}, the slight difference (<1 W m^{-2}, Table 5) between the BULK and the SLUCM (Figs. 5e,g) is due to the changes in surface albedo under different urban parameterizations. For BULK, Q_{LW} loss over rural areas is smaller than that over urban areas (Fig. 5f) because of lower surface temperature over rural areas (Fig. 4). In the SLUCM, warmer surface temperatures over the urban areas lead to a higher outgoing longwave radiation at the surface (not shown). However, incoming longwave radiation at the surface also increases due to warmer atmospheric temperatures in the lower troposphere (Fig. 3). As a result, Q_{LW} over all three urban areas is similar in the SLUCM (Fig. 5h). In addition to the surface heat flux components, the extent to which advection modulates the near-surface conditions is estimated next.

4. Role of temperature and momentum advection

To understand the role of temperature and momentum advection over the Houston area, we divide the region into windward and leeward sides based on the prevailing winds (Fig. 6) that are predominantly from southeast to northwest. Thus, we consider the southeastern part of the urban area as the windward side and the northwestern part of the urban area as the leeward side.

a. Role of temperature advection

The horizontal temperature advection in the BULK and SLUCM is shown in Fig. 7. We show the results at the lowest model level (~50 m) because this is the first level up from the surface where all the variables are available to compute temperature and momentum advection. Over the rural areas in the BULK scheme, negative temperature advection peaks around 1900 UTC 25 August 2000 in the windward side of the urban areas (Fig. 7c) before decreasing to nearly zero around 0200 UTC and remaining steady after that. On the leeward side of the urban areas, the evolution of advection is very similar,

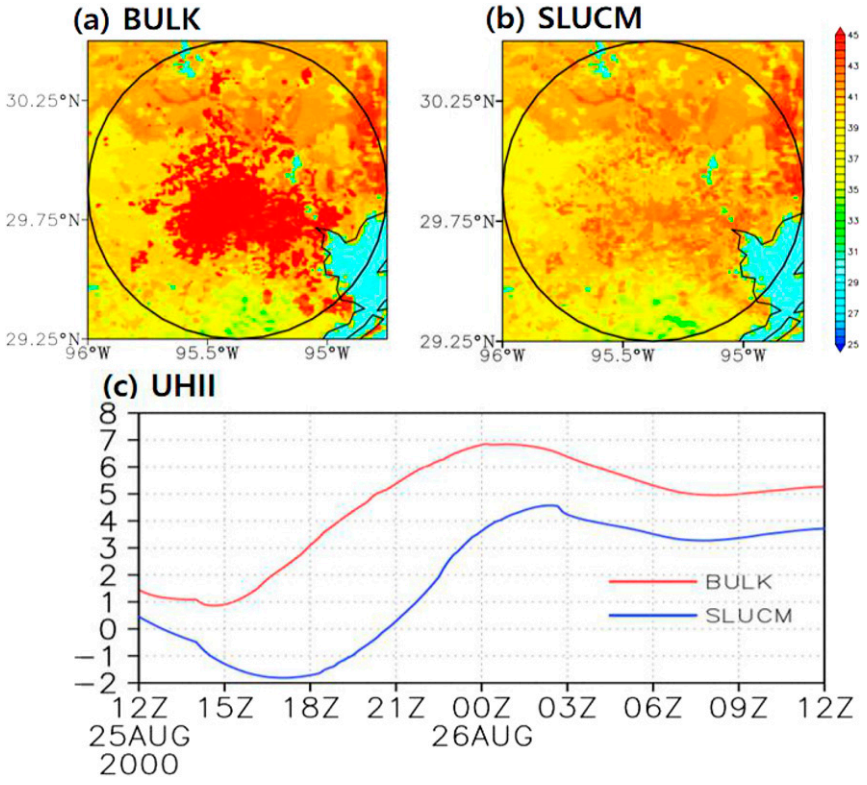

FIG. 4. Surface skin temperature (°C) in Houston at 1900 UTC (1300 local time) 25 Aug 2000 from the (a) BULK and (b) SLUCM. Also shown is (c) urban heat island intensity (UHII; °C) calculated as skin temperature over urban areas (LIR and COI/HIR) minus rural areas over the circled areas in (a) and (b).

but with a time offset, as expected, of about 3 h (Fig. 7, left). Over the windward side (Fig. 7d), the peak in negative temperature advection appears around 0000 UTC 26 August. In the BULK simulations, the slope of the temperature advection resembles the slope of the local tendency, suggesting that the horizontal advection of temperature is an important factor in the local change in temperature. In the SLUCM, however, temperature advection (Fig. 7, right, blue) is small on both sides of the urban area compared to BULK and does not seem to play a significant role in local temperature tendency, indicating that the surface heat flux mostly drives the near-surface temperature in the SLUCM simulations. Temperature tendency in the SLUCM simulations is determined by the surface heat flux, whereas in the BULK simulations, temperature advection plays a vital role along with the surface heat flux. This result is consistent with Figs. 2 and 4, where the increase in temperature in the BULK over the urban areas was much more than the SLUCM, leading to a stronger temperature gradient and hence stronger advection of temperature in the presence of onshore winds (Figs. 3 and 6). What changes the winds in and around the urban area is analyzed next using a momentum budget analysis.

b. Role of momentum advection

The momentum budget equations are widely used in large-scale studies to understand the processes that control winds (e.g., Carr and Bretherton 2001; Lin et al. 2005; Ray and Zhang 2010). The zonal and the meridional momentum budget equations in pressure coordinates are given by

$$\frac{\partial u}{\partial t} = -u\frac{\partial u}{\partial x} - v\frac{\partial u}{\partial y} - \omega\frac{\partial u}{\partial p} - \frac{\partial \phi}{\partial x} + fv + R \quad \text{and} \tag{1}$$

$$\frac{\partial v}{\partial t} = -u\frac{\partial v}{\partial x} - v\frac{\partial v}{\partial y} - \omega\frac{\partial v}{\partial p} - \frac{\partial \phi}{\partial y} + fu + R, \tag{2}$$

where (u, v, ω) is the three-dimensional wind vector, ϕ is the geopotential, f is the Coriolis parameter, and R is the residual. The residual here represents friction, other subgrid-scale processes, and errors in the data and calculation. The term on the left-hand side is the local tendency. The first three terms on the right-hand side are the advective terms by the zonal, meridional, and vertical winds, respectively, and the fourth and the fifth terms are the pressure gradient and the Coriolis term. Here, we present an analysis of the momentum budget at the lowest model level (~50 m) because this is the first level up from the surface where all the variables are available to compute the momentum budget.

To represent the terms conveniently, we merge the vertical advection (VADV) and the residual R into one term (labeled here VADV + R) and the pressure gradient and Coriolis into another term (labeled here $P + C$). This merging of terms was done to isolate any possible influence from the horizontal

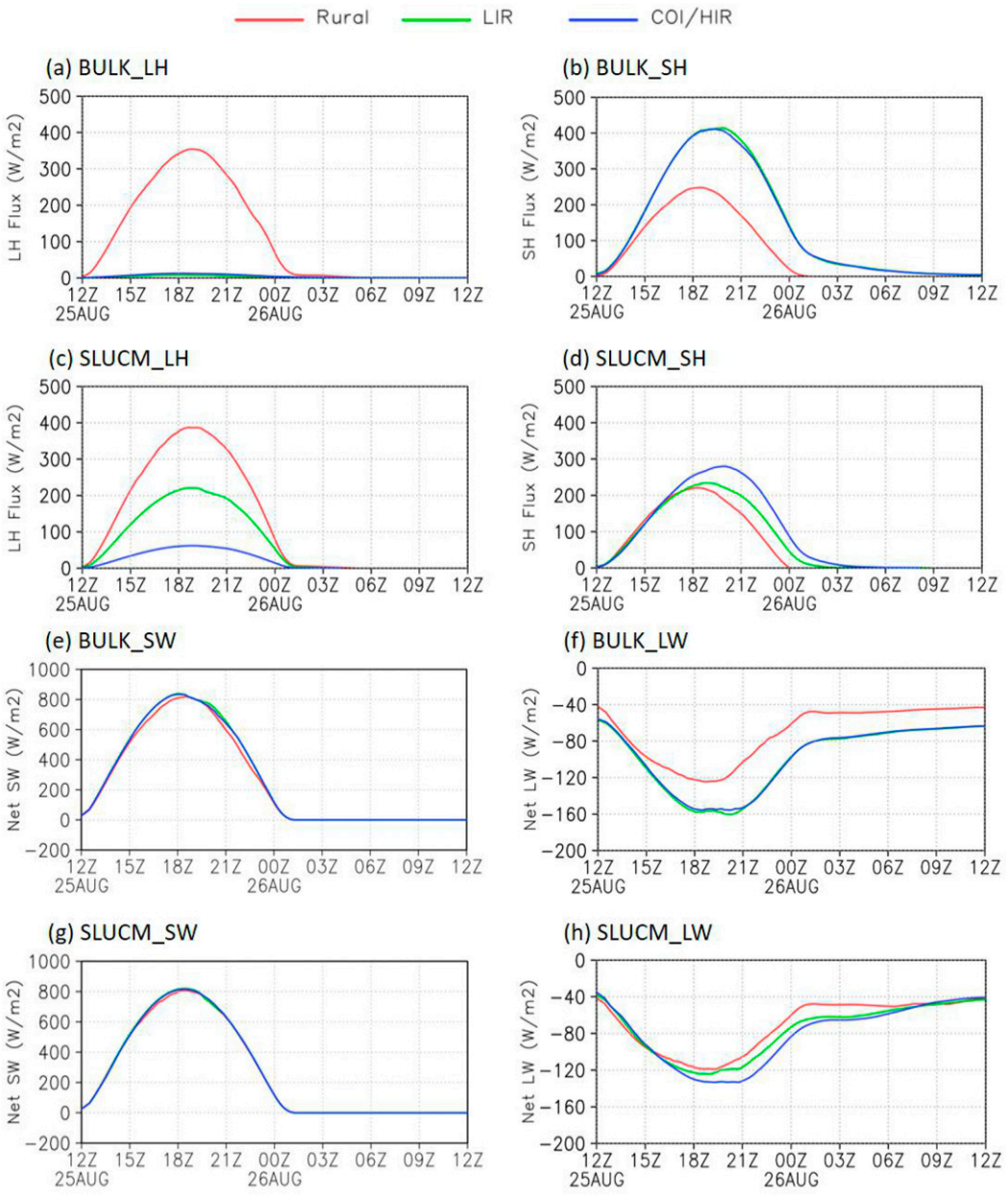

FIG. 5. Surface (a),(c) Q_{LH}; (b),(d) Q_{SH}; (e),(g) Q_{SW}; and (f),(h) Q_{LW} (W m^{-2}) for all land categories.

advection (HADV), given that large temperature gradients are found between rural and urban areas (Figs. 3 and 4). For the zonal momentum budget (Fig. 8), the local tendency has two peaks over the northwestern rural areas in both BULK (Fig. 8a) and SLUCM (Fig. 8c), but the peaks are less prominent in southeastern rural areas (Figs. 8c,g). The peak in forcing from pressure gradient in the northern rural areas (Figs. 8a,e) lags that in southern rural areas (Figs. 8c,g) by 2–3 h. The increase in the local tendency of zonal wind from 2100 UTC 25 August to 0300 UTC 26 August 2000 over the urban areas is similar to the HADV (Fig. 8, right) indicating the importance of HADV in modulating the peak zonal winds over the urban areas. The lag in peak zonal winds between the northwestern and southeastern urban areas is about 1–2 h. The $P + C$ has a smoother variation and seems to have little to no time lag between the northwestern and southeastern urban areas (Fig. 8, right, blue). The VADV + R seems to be most important between 1200 and 1800 UTC 25 August.

The terms of the zonal momentum budget during day and night are shown in Fig. 9. The daytime (2100 UTC 25 August–0000 UTC 26 August) and nighttime (0000 UTC to 0300 UTC 26 August) periods were chosen based on the timing of peak winds (Fig. 2, bottom panels), which is at about 0000 UTC 26 August before declining (Fig. 2). As a result, we wanted to

TABLE 5. The surface heat flux components (W m^{-2}) from 1200 UTC (0600 LST) 25 Aug to 1200 UTC (0600 LST) 26 Aug 2000 over rural, LIR, and COI/HIR areas.

	Sensible heat flux Q_{SH}			Latent heat flux Q_{LH}			Net longwave Q_{LW}			Net shortwave Q_{SW}		
PBL	Rural	LIR	COI/HIR	Rural	LIR	COI/HIR	Rural	LIR	COI/HIR	Rural	LIR	COI/HIR
						BULK						
Ensemble	68.6	142.3	139.9	108.4	2.7	4.5	68.5	95.8	94.7	248.3	263.2	260.8
YSU	68.3	138.8	138.1	101.5	2.0	3.1	73.1	98.6	98.4	246.0	263.7	263.7
MYJ	68.1	141.7	140.4	111.7	4.6	7.0	68.2	95.4	94.3	250.0	264.1	264.0
MYNN	68.7	147.9	141.6	109.2	0.3	2.8	65.6	94.8	92.5	246.5	263.9	255.3
BouLac	69.4	140.8	139.7	111.1	3.9	5.1	67.0	94.3	93.5	250.8	261.2	260.4
						SLUCM						
Ensemble	57.0	72.8	89.8	117.5	69.7	19.5	67.8	74.2	78.1	248.0	255.0	252.4
YSU	51.4	75.0	92.0	103.7	67.2	18.8	73.4	81.8	84.7	245.6	255.6	250.8
MYJ	61.3	72.5	89.4	121.1	70.5	19.6	67.5	72.7	76.7	251.4	255.9	253.3
MYNN	58.9	71.2	88.6	122.0	70.7	19.6	65.0	70.1	74.8	245.5	253.0	251.5
BouLac	56.3	72.4	89.5	123.2	70.7	19.8	65.4	72.2	76.3	245.6	255.5	254.1

find the factors that contribute to the simulated peak winds. In the rural area (Fig. 9, left), local tendency of zonal winds is dominated by the $P + C$ during both late afternoon and evening. Over rural areas, HADV and VADV + R seem to be opposite in sign compared to local tendency of zonal winds for both the BULK and SLUCM simulations. Over urban areas, during the late afternoon, HADV in BULK has the same sign as that of local tendency of zonal winds (Figs. 9b,d). In the northwestern urban area, during the late afternoon (Figs. 9b,f), although VADV + R has similar sign and magnitude to that of local tendency in zonal winds, fluctuation in VADV + R do not match the fluctuation in local tendency (Figs. 8b,f). On the other hand, over all of the urban areas (Fig. 9, right), HADV seems to be important for zonal winds, and is further evidenced by its covariation with local tendency of zonal winds (Fig. 8, right). At evening, over urban areas (Fig. 9, right, green), HADV and $P + C$ control the local tendency of zonal momentum, with HADV playing a bigger role in the southeastern urban area (Figs. 8d,h) and $P + C$ playing a bigger role in the northwestern urban area (Figs. 8b,f).

The temporal variation of the terms in the meridional momentum budget (Fig. 10) and the magnitude of terms during

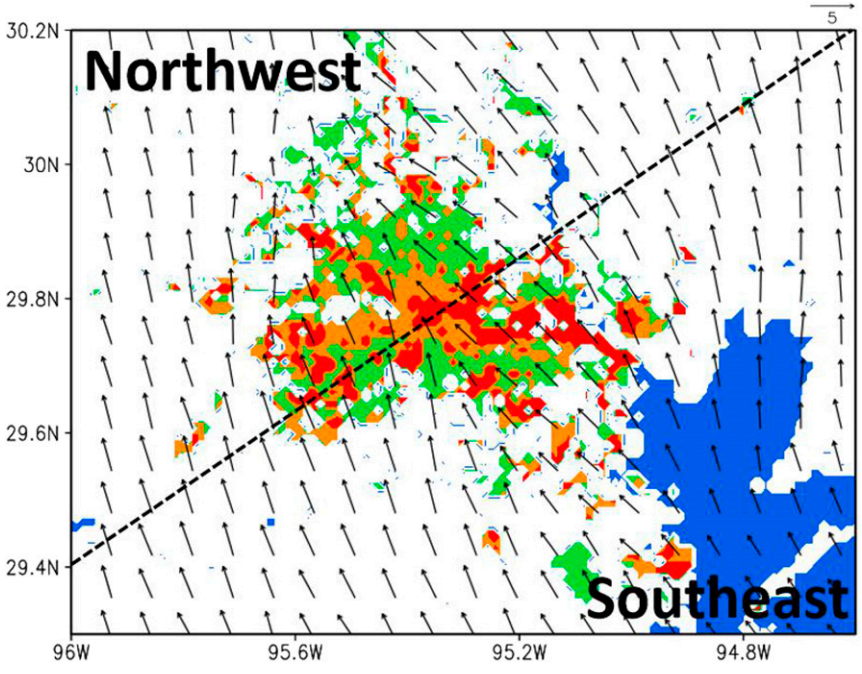

FIG. 6. Winds (vectors; m s^{-1}) at the lowest model level (~50 m) over the Houston area averaged from 1800 UTC 25 Aug to 0600 UTC 26 Aug 2000. The shading indicates the land-use category of rural (white), LIR (green), HIR (orange), and COI (red) areas. Water bodies are marked in blue. The black dashed line divides this area into windward (southeast) and leeward (northwest) sides of the city.

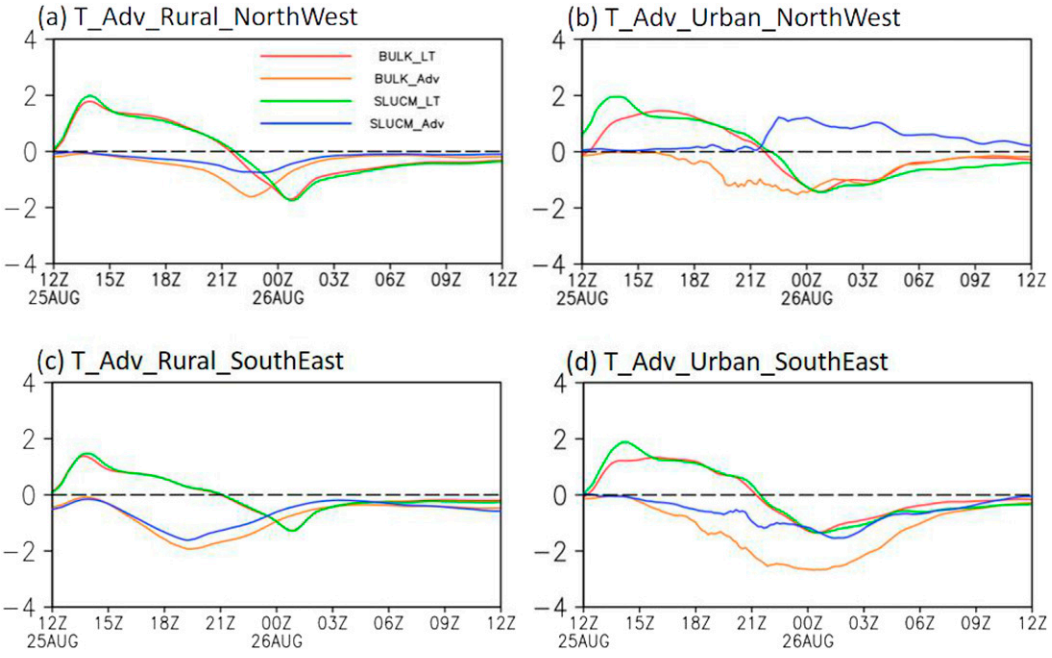

FIG. 7. The local tendency and horizontal advection of temperature (K h^{-1}) from the BULK and the SLUCM averaged over all simulation points in the (left) rural and (right) urban (LIR and COI/HIR) land categories. The legends in (a) apply to all panels. The (a),(b) northwest and (c),(d) southeast represent the leeward and windward areas that are separated by the black dashed line in Fig. 6.

late afternoon and evening (Fig. 11) both show a clear relationship between the local tendency (black) and HADV (red) of meridional winds. Over the rural areas, HADV is small in the morning (before 1800 UTC 25 August) and at night (after 0600 UTC 26 August). However, during late afternoon and evening (1800 UTC 25 August to 0600 UTC 26 August), HADV plays a role along with $P + C$ in variation of local tendency of meridional winds. Over the southeastern urban areas (Figs. 10d,h), the peak local tendency of meridional winds between 1800 and 2100 UTC 25 August 2000 is similar to the HADV. A similar trend can be seen for the northwestern urban areas as well, in particular for BULK (Fig. 10b). A temporal offset of 1–2 h between the southeastern and northwestern urban areas in local tendency, $P + C$, and HADV can also be noticed, and is consistent with the large-scale wind patterns (Figs. 3 and 6). Further quantification of the relative influence of the terms of the meridional momentum budget during the peak winds is given in Fig. 11. In the northwestern rural areas (Figs. 11a,e), HADV along with $P + C$ seem to dominate local tendency and is further confirmed by their high correlations with local tendency (Fig. 12a). In the northwestern urban area, similar results are found where HADV and $P + C$ are important (Figs. 11b,f) for meridional momentum budget, and this is further confirmed by their higher correlations with local tendency (Figs. 12a,b, red). In the southeastern urban area, correlation between HADV and local tendency of meridional winds is found to be higher in SLUCM than in the northwestern urban area (Fig. 12, right). Note that, even though $P + C$ has a greater magnitude than HADV for most cases in Fig. 10, the temporal variation in $P + C$ is small (see blue lines in Fig. 10) and forms the baseline upon which variation in HADV may explain the variation in local tendency. As a result, the HADV in the meridional momentum equation seems to be the dominant term in determining the evolution of near-surface winds at their peak during the simulation period, particularly in the southeastern urban areas (Figs. 10d,h).

5. Sensitivity to the urban and PBL schemes

In this section, we discuss the sensitivity of the results presented in earlier sections to different urban and PBL schemes. A detailed analysis of the reasons behind the differences among the urban and PBL schemes is beyond the scope of this paper.

a. Sensitivity to the urban schemes

Here we show how robust the differences between the two types of urban simulations are regardless of the used PBL scheme. The T2 is always higher in BULK than that in SLUCM irrespective of the PBL scheme used (Fig. 13, top). A similar trend is also found for W10 (Figs. 13e–h), except under the YSU scheme, where the peak winds are higher in SLUCM than in BULK. Huang et al. (2019) in their work on sensitivity of urban boundary layer simulation to urban canopy models and PBL schemes found that the simulated 2-m temperature and 10-m winds are more sensitive to UCMs than PBL schemes. Wang et al. (2019) studied the effects of urban parameterization on the passage of cold front during a pollution episode using the BULK and SLUCM urban schemes. They found

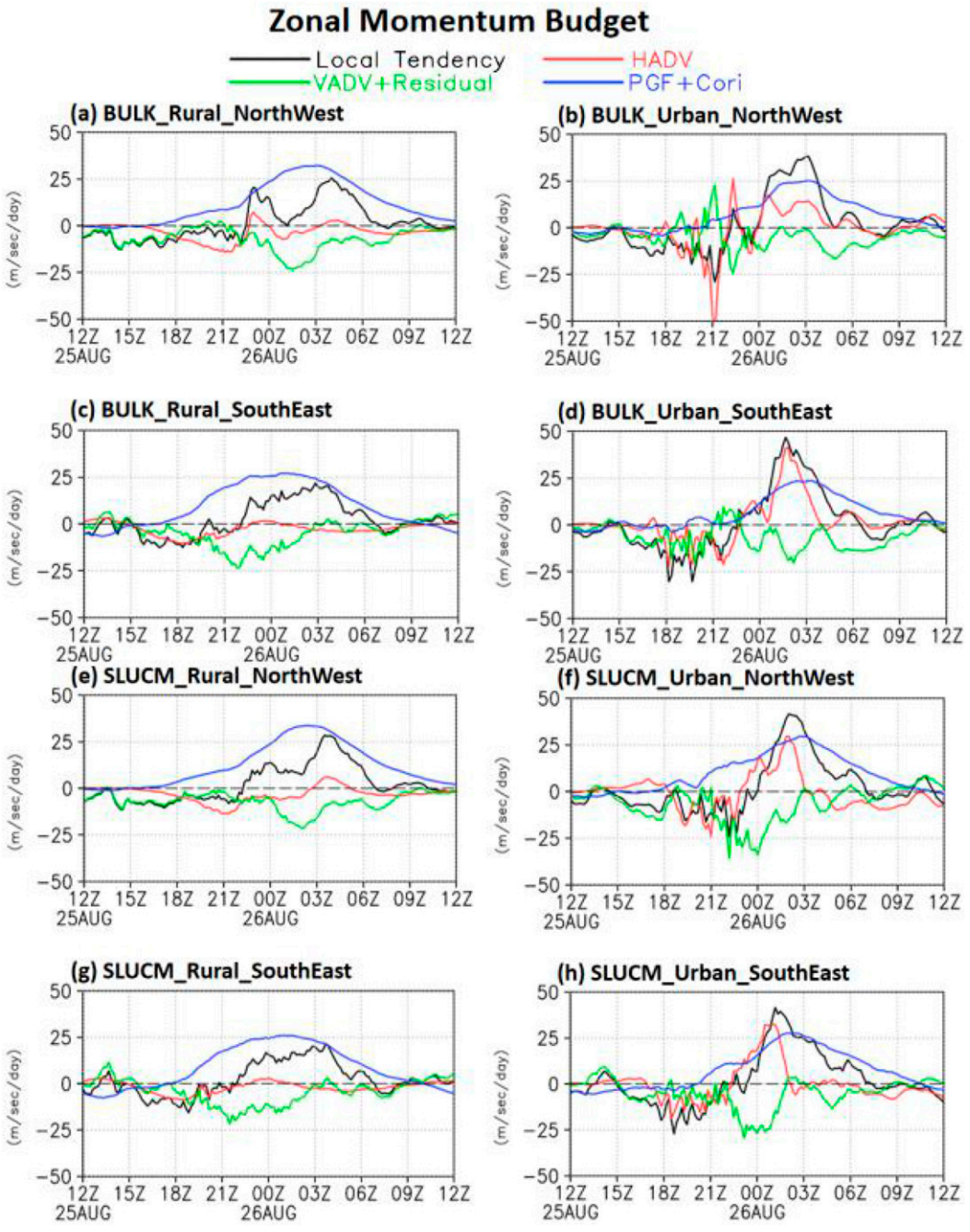

FIG. 8. The terms of the zonal momentum budget ($m\,s^{-1}\,day^{-1}$) for the BULK and SLUCM averaged over all simulation points in (a),(c),(e),(g) rural and (b),(d),(f),(h) urban (LIR and COI/HIR) land categories. The acronyms are defined in the text. Northwest and southeast represent the leeward and windward areas that are separated by the black dashed line in Fig. 6.

improvement in the temperature and relative humidity using SLUCM under higher urbanization levels, and wind speed simulation was better in the rural areas. The simulated latent heat flux (Figs. 13i–l) is higher, but the simulated sensible heat flux (Figs. 13m–p) is lower in SLUCM than BULK under all PBL schemes with varying magnitudes. Over rural areas, the difference in latent and sensible heat flux between the BULK and SLUCM is small compared to that in the urban areas and is consistent under all PBL schemes (Table 5).

For all urban configurations, the simulated winds are generally lower than the observations in the morning, but during the early evening and overnight periods, they are higher than observations. Over the 24-h period, the averaged simulated winds were higher than observations (see

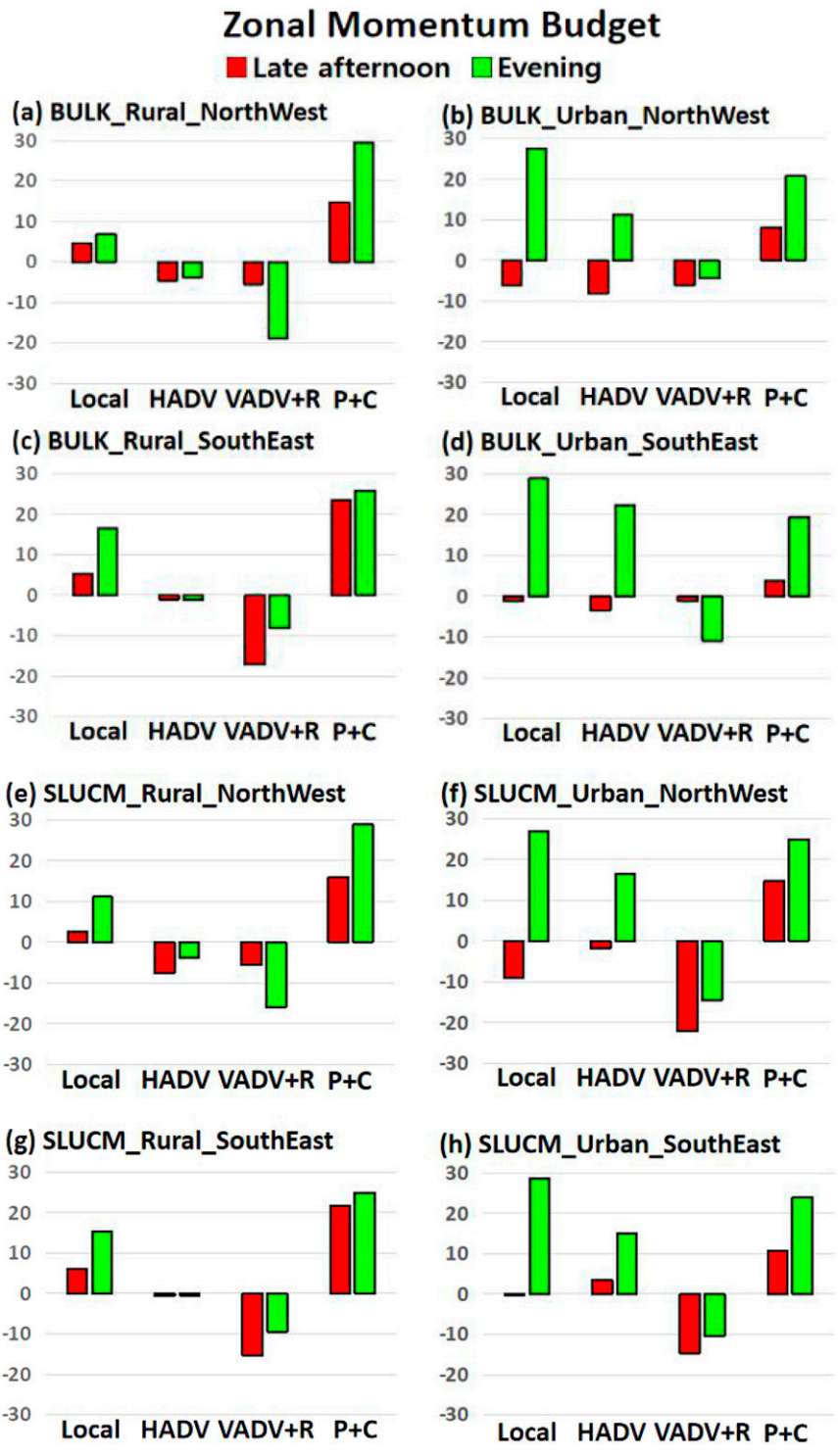

FIG. 9. The terms in zonal momentum budget ($m\,s^{-1}\,day^{-1}$) from BULK and SLUCM averaged during the late afternoon (red; averaged from 2100 UTC 25 Aug to 0000 UTC 26 Aug) and evening (green; averaged from 0000 UTC to 0300 UTC 26 Aug 2000) and averaged over all simulation points in (a),(c),(e),(g) rural and (b),(d),(f),(h) urban (LIR and COI/HIR) land categories. The acronyms are defined in the text. Northwest and southeast represent the leeward and windward areas that are separated by the black dashed line in Fig. 6.

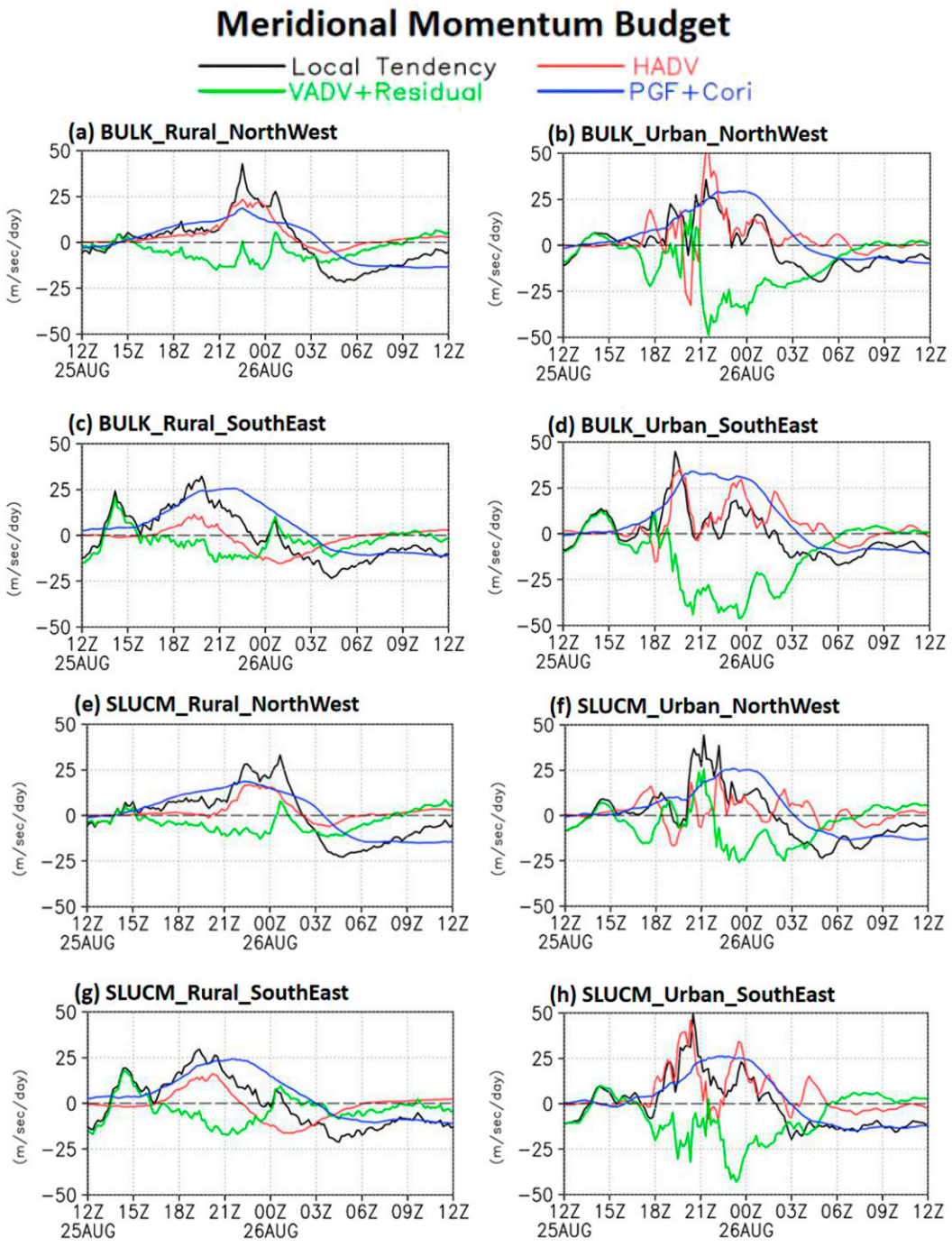

FIG. 10. As in Fig. 8, but for the meridional momentum budget.

Tables 2–4). This result is consistent with Shimada et al. (2011), who found that all of the available PBL schemes (in WRF 3.3) produced a positive mean bias for the near-surface wind speed. They attributed this to a systematic error in the WRF Model. Within the urban land categories, linear correlations between model and observed wind speed are primarily between 0.85 and 0.95. The lower correlation between simulated and observed W10 compared to T2 is mainly due to a phase difference between the simulated and observational W10 in the afternoon with model W10 peaking about an hour later than the observed W10.

b. *Sensitivity to the PBL schemes*

In the BULK simulations, the nonlocal YSU PBL scheme performs better in capturing the near-surface temperature and winds than the three local schemes (Table 2–4). In the presence

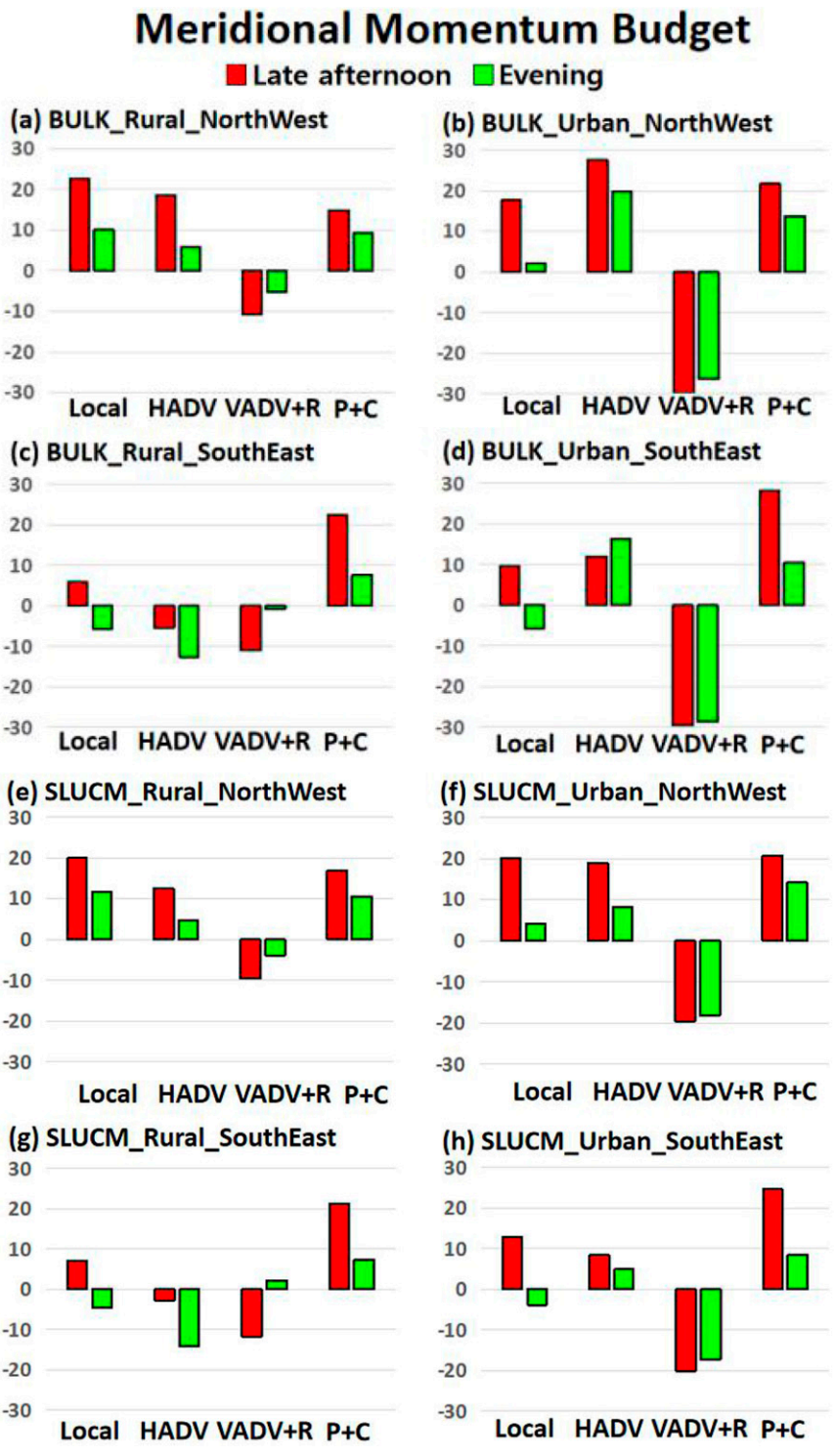

FIG. 11. As in Fig. 9, but for the meridional momentum budget.

of strong surface heating, the performance of the nonlocal YSU scheme is not surprising since the YSU scheme is well suited to conditions with strong daytime heating (Hu et al. 2010, 2013; Shin and Hong 2011; Kolling et al. 2012; Xie et al. 2012). However, in the SLUCM simulations, the Bougeault–Lacarrere (BouLac) scheme performs best over rural (RMSE of 0.53°C) and COI/HIR (RMSE 0.79°C) areas, but MYJ performs best over the LIR. For the LIR (Table 3) and

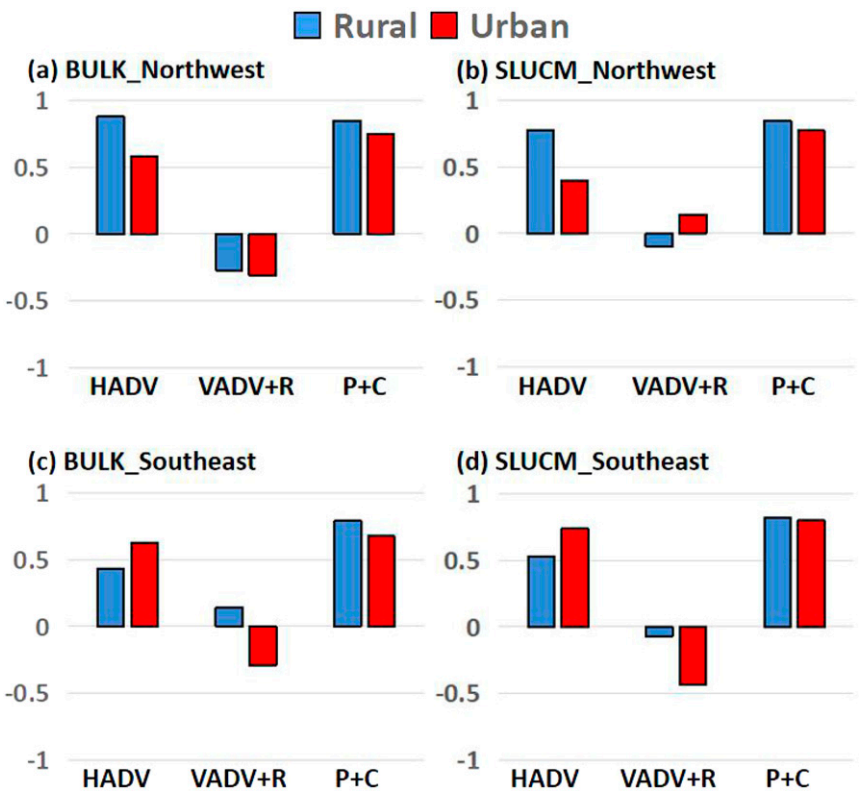

FIG. 12. Correlation in meridional momentum budget terms between local tendency term and HADV, VADV + R, and P + C for the (a),(c) BULK and (b),(d) SLUCM over rural (blue) and urban (red, LIR and COI/HIR) areas from 1200 UTC 25 Aug to 1200 UTC 26 Aug; (top) northwest and (bottom) southeast represent the leeward and windward areas that are separated by the black dashed line in Fig. 6.

COI/HIR (Table 4) land categories, the YSU scheme has the largest RMSE. Most of this error is associated with the poor performance of the YSU scheme during the nighttime when it overestimates the amount of cooling in the city. Near-surface temperatures from PBL schemes and observations have correlation coefficients between 0.95 and 1.00, indicating that all the PBL schemes and urban configurations reasonably capture the diurnal pattern of T2.

For near-surface winds in BULK simulations, the YSU scheme provides the most accurate near-surface winds over urban areas, whereas all the locally driven PBL schemes produce winds that are higher than the observations (Tables 3 and 4). Our results are consistent with Shin and Hong (2011), who showed that the YSU scheme tends to perform best in unstable atmospheric conditions, and local PBL schemes tend to perform better in stable conditions. In the SLUCM simulations, this trend reverses: the YSU scheme provides the least-accurate wind speeds within the urban environment during the daytime.

For surface latent and sensible heat fluxes, most of the differences among the PBL schemes originate during the daytime. The magnitudes of these terms have very little variation among the three local schemes. The only nonlocal scheme (YSU) overestimates surface sensible heat flux over the COI/HIR areas compared to the local schemes, due to higher skin temperature in the YSU. The PBL schemes have little to no effect on the surface radiative fluxes in either the BULK or the SLUCM simulations (Table 5) because the forecast period did not have moist convection or clouds. Thus, the cloud-radiation effect did not change much between the simulations. In all simulations, the YSU scheme has the maximum amount of longwave heat loss from the surface, as the skin temperature was higher in the YSU than other PBL schemes. This difference is especially noticeable in the SLUCM simulations. There is a little variation in the local tendency of temperature and horizontal temperature advection in BULK simulations using different PBL schemes over urban areas. Over the rural areas during the daytime, temperature advection was found to be higher in the local schemes than the YSU scheme due to a larger urban–rural temperature gradient.

The sensitivity of the zonal momentum budget to the PBL schemes is shown over the urban areas (Fig. 14) only because there is much less variability among the PBL schemes over rural areas. In the BULK and SLUCM parameterizations (Fig. 14), all PBL schemes show very similar results in the evening (Fig. 14, green), with larger differences during late afternoon (Fig. 14, red). The YSU and MYJ results are similar for all cases except for local tendency term in SLUCM during

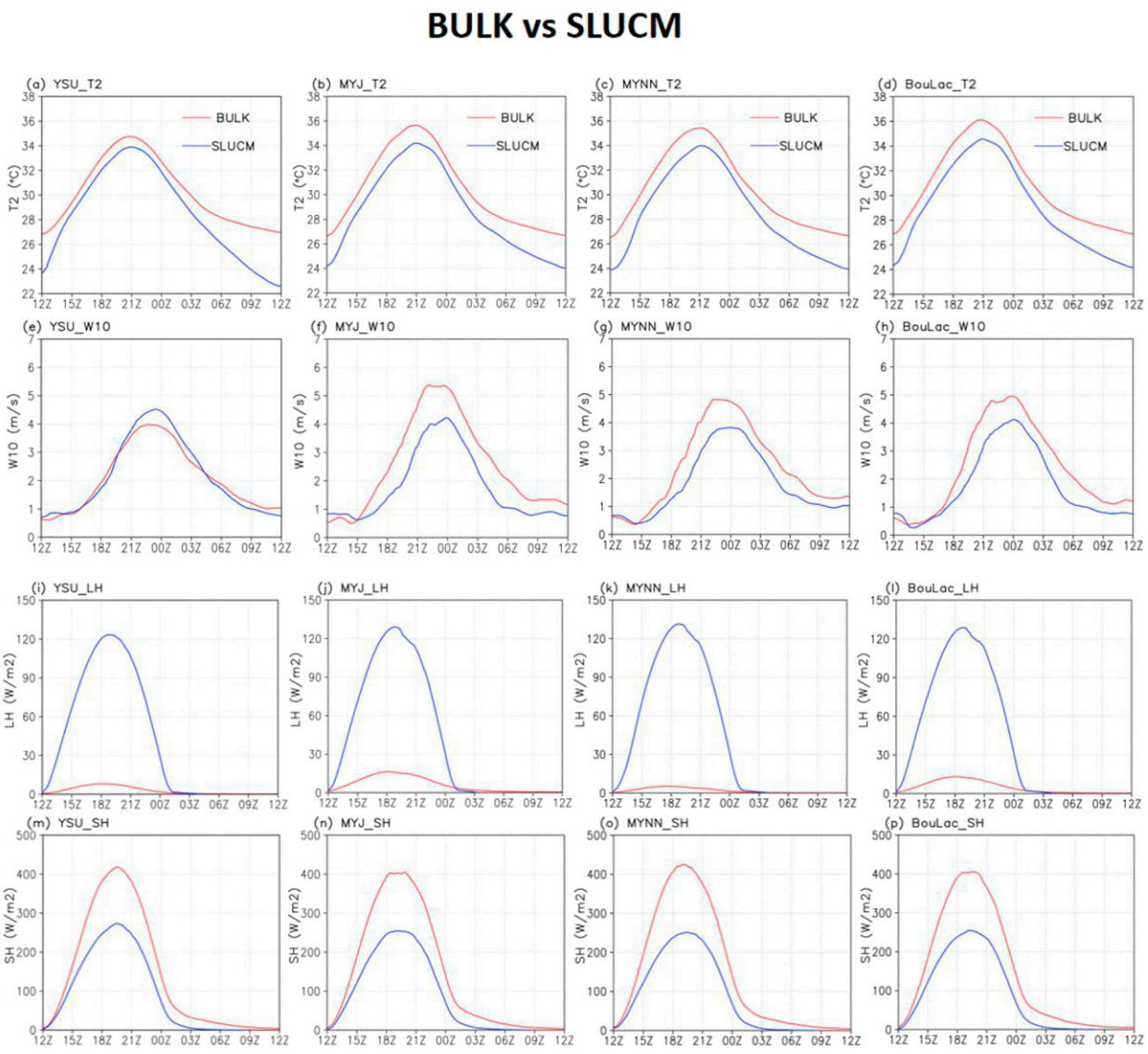

FIG. 13. (a)–(d) 2-m temperature (T2; °C), (e)–(h) 10-m winds (W10; m s^{-1}), (i)–(l) surface latent heat flux (W m^{-2}); and (m)–(p) surface sensible heat flux (W m^{-2}) over all urban land category from the BULK (red) and the SLUCM (blue) simulations under the four different PBL schemes: (left) YSU, (left center) MYJ, (right center) MYNN2, and (right) BouLac.

daytime (Fig. 14b). In the meridional momentum budget using the BULK parameterization (Fig. 15, left), all the terms are similar in different PBL schemes, particularly during the late afternoon. In the evening, local tendencies are small (Fig. 15, top, green). The HADV in BULK has larger variation in PBL schemes (Fig. 15c) than in SLUCM (Fig. 15d). In both the BULK and SLUCM, all PBL schemes show positive HADV (Figs. 15c,d), negative VADV + R (Figs. 15e,f), and positive $P + C$ (Figs. 15g,h) in both the late afternoon and evening.

Overall, note that, on a particular day, a particular scheme can seem to perform well because of cancellation of errors (e.g., Sharma et al. 2016). As a result, our analysis based on a 24-h time period should be treated with caution. To avoid the sensitivity of the results to the PBL schemes, we used the ensemble mean of the four simulations using four different PBL schemes. More important, model performance should be treated as a performance indicator of a set of schemes as has been done in several previous studies (e.g., Bhattacharya et al. 2018; Lamraoui et al. 2019; Schwitalla et al. 2020), and not as a performance validation of a particular scheme. Such an analysis, however, is beyond the scope of this paper.

6. Summary and conclusions

The role of advection of heat and momentum on the near-surface temperature and winds is evaluated over windward and leeward sides of Houston during a 24-h period in August 2000 that was marked by dry conditions (Nielsen-Gammon 2002; Cheng and Byun 2008). Two sets of experiments were conducted, one using the default urban scheme (BULK) and one

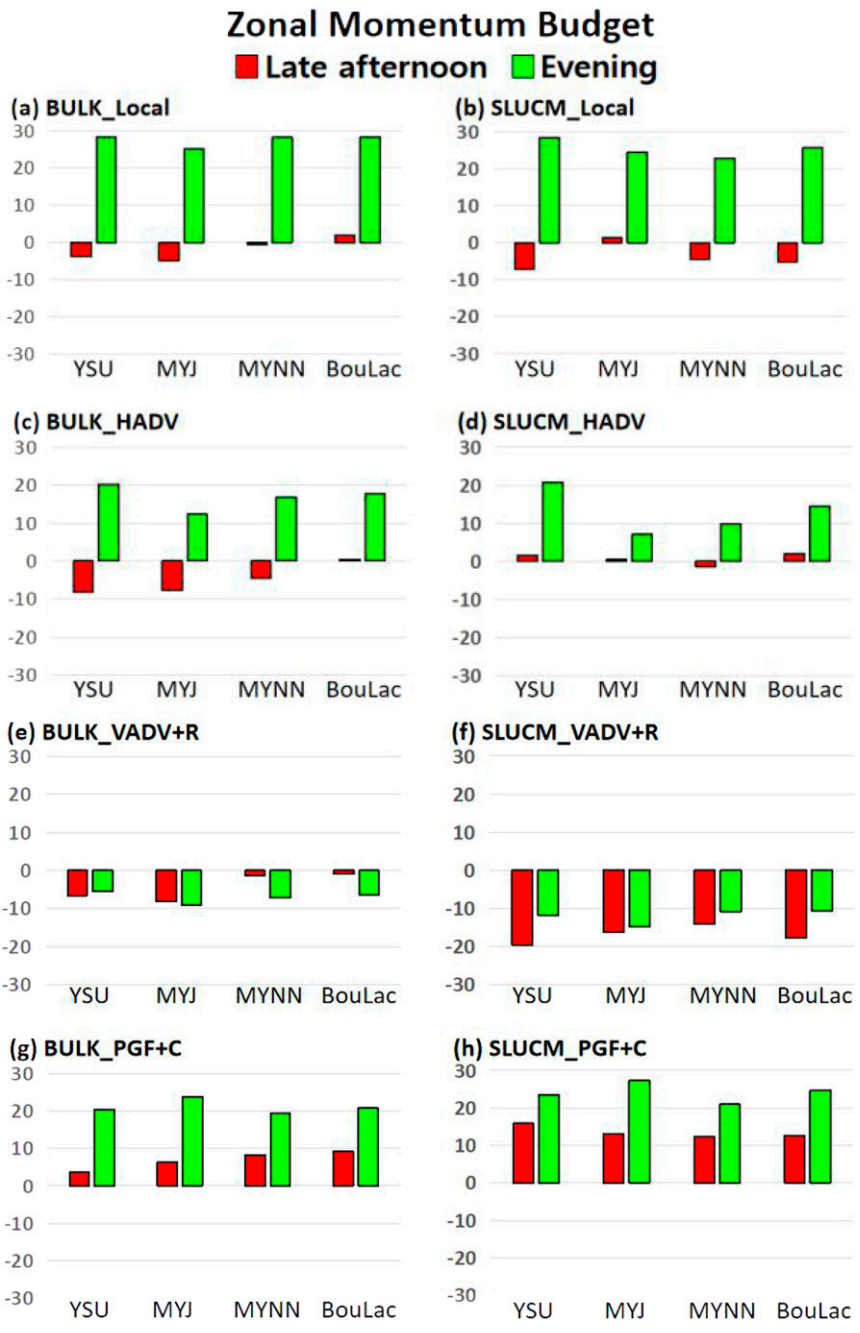

FIG. 14. Zonal momentum budget ($m\,s^{-1}\,day^{-1}$) from different PBL schemes in (a),(c),(e),(g) BULK and (b),(d),(f),(h) SLUCM simulations over all simulation points in the urban land category. Late afternoon is from 2100 UTC 25 Aug to 0000 UTC 26 Aug, and evening is from 0000 UTC to 0300 UTC 26 Aug 2000.

using the single-layer urban canopy model (SLUCM) available within the WRF Model. Each experiment consists of four simulations using four widely used planetary boundary layer schemes (YSU, MYJ, MYNN, and BouLac; Table 1). Previous studies have rarely been conducted based on an ensemble of simulations, likely because of computational expenses. The main results and implications of this study are as follows:

(i) Our results show that the horizontal advection of 2-m temperature (Fig. 7) seems to be an important factor in the BULK scheme because of a larger 2-m temperature gradient in the presence of warmer temperatures over urban areas (Figs. 3 and 4). In the SLUCM scheme, horizontal advection of temperature is small (Fig. 7) in the presence of a smaller temperature gradient (Fig. 4),

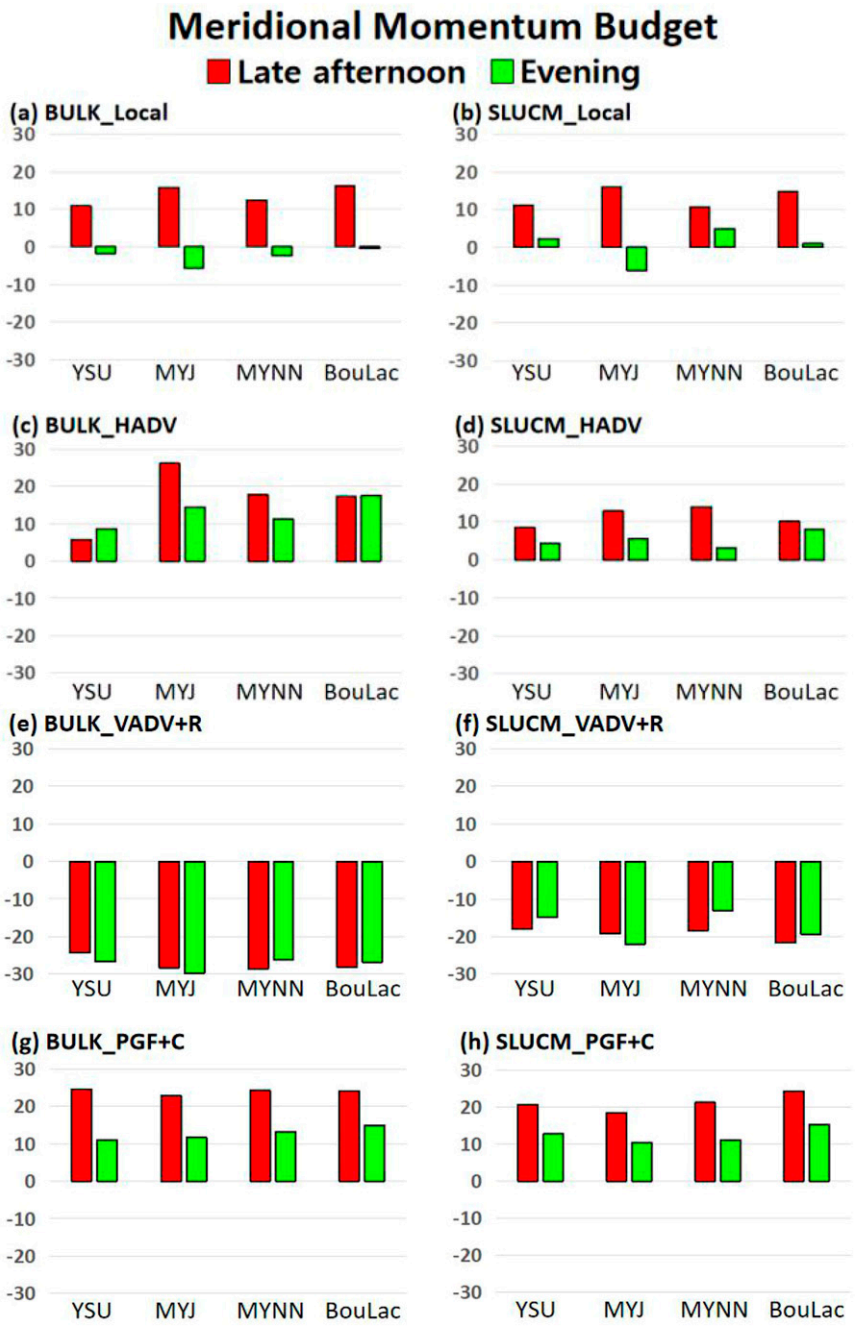

FIG. 15. As in Fig. 14, but for the meridional momentum budget.

and the 2-m temperature is determined by the skin temperature and surface heat flux.

(ii) Previous studies have largely ignored any quantitative analysis regarding the impacts of momentum advection within an urban area due to the use of different urban parameterizations or PBL schemes. An analysis of the momentum budget shows that even though pressure gradient and Coriolis are the largest terms, horizontal advection of meridional momentum plays a prominent role during the peak near-surface winds, and this effect is more pronounced on the windward side of the city. The local tendency in winds in the leeward side lags that in the windward side by about 1–2 h, but little to no time lag is found in pressure gradient and Coriolis.

(iii) The peak 10-m winds are influenced by the horizontal advection of momentum over urban areas (Figs. 8–11), although the extent of influence varies among the PBL schemes (Figs. 14 and 15). Also, our simulations using the

BULK (Fig. 3b) and the SLUCM (Fig. 3c) schemes clearly show the modulation of winds due to the urban areas and were found to be consistent under all PBL schemes. Whether this result was less sensitive to the PBL schemes because of the coarse vertical resolution (35 layers) of the simulations cannot be ruled out. The near-surface winds in the reanalysis (ERA-Interim) data were southerly over Houston (Fig. 3). The reanalysis winds were not modulated by the urban areas possibly because of the coarse resolution of the reanalysis grid and the lack of a more sophisticated urban scheme in the reanalysis model system. Therefore, near-surface reanalysis products should be treated with caution in urban areas and their surroundings.

(iv) Our simulation period was marked by light winds and dry conditions over Houston. Yet, the role of momentum advection on the variability of winds could not be ignored. Therefore, in an urban atmosphere with moist convection, momentum advection is expected to play a much greater role in variation in winds. Of course, the results will be dependent on various other factors, such as the large-scale winds, orientation of the coastlines, and shape and extent of the cities.

In summary, our results quantified the influence of advection on the near-surface temperature and winds over an urban area under different urban and PBL schemes. The results indicate that proper representation of land-use patterns with sophisticated urban parameterization is essential to capture the variation in near-surface temperature and wind that are important in determining the UHI intensity.

Acknowledgments. The simulations were conducted using the "Blueshark" computer clusters, funded by the National Science Foundation (NSF) at the Florida Institute of Technology. This work was partially supported by a grant from the ONR (N00014-16-1-3091) to author Ray. We thank Jimy Dudhia and three anonymous reviewers for their constructive comments that significantly improved the paper.

REFERENCES

Banks, R. F., J. Tiana-Alsina, J. M. Baldasno, F. Rocadenbosch, A. Papayannis, S. Solomos, and C. G. Tzanis, 2016: Sensitivity of boundary-layer variables to PBL schemes in the WRF model based on surface meteorological observations, lidar, and radiosondes during the HygrA-CD campaign. *Atmos. Res.*, **176–177**, 185–201, https://doi.org/10.1016/j.atmosres.2016.02.024.

Bassett, R., X. Cai, L. Chapman, C. Heaviside, J. E. Thornes, C. L. Muller, and E. L. Warren, 2016: Observations of urban heat island advection from a high-density monitoring network. *Quart. J. Roy. Meteor. Soc.*, **142**, 2434–2441, https://doi.org/10.1002/qj.2836.

——, ——, ——, ——, and ——, 2017: The effects of heat advection on UK weather and climate observations in the vicinity of small urbanized areas. *Bound.-Layer Meteor.*, **165**, 181–196, https://doi.org/10.1007/s10546-017-0263-0.

Belcher, S. E., O. Coceal, E. V. Goulart, A. C. Rudd, and A. G. Robins, 2015: Processes controlling atmospheric dispersion through city centers. *J. Fluid Mech.*, **763**, 51–81, https://doi.org/10.1017/jfm.2014.661.

Best, M. J., 2005: Representing urban areas within operational numerical weather prediction models. *Bound.-Layer Meteor.*, **114**, 91–109, https://doi.org/10.1007/s10546-004-4834-5.

Bhattacharya, R., S. Bordoni, K. Suselj, and J. Teixeira, 2018: Parameterization interactions in global aquaplanet simulations. *J. Adv. Model. Earth Syst.*, **10**, 403–420, https://doi.org/10.1002/2017MS000991.

Bornstein, R. D., and S. D. Johnson, 1977: Urban-rural wind velocity differences. *Atmos. Environ.*, **11**, 597–604, https://doi.org/10.1016/0004-6981(77)90112-3.

Bougeault, P., and P. Lacarre're, 1989: Parameterization of orography induced turbulence in a mesobeta–scale model. *Mon. Wea. Rev.*, **117**, 1872–1890, https://doi.org/10.1175/1520-0493(1989)117<1872:POOITI>2.0.CO;2.

Brownlee, J., 2016: Evaluation of near-surface temperature and wind speed using the new single-layer urban canopy model in Houston. M.S. thesis, Department of Marine and Environmental Systems, Florida Institute of Technology, 137 pp.

——, P. Ray, M. Tewari, and H. Tan, 2017: Relative role of turbulent and radiative flux on the near-surface temperature in a single-layer urban canopy model over Houston. *J. Appl. Meteor. Climatol.*, **56**, 2173–2187, https://doi.org/10.1175/JAMC-D-17-0088.1.

Carr, M. T., and C. S. Bretherton, 2001: Convective momentum transport over the tropical Pacific: Budget estimates. *J. Atmos. Sci.*, **58**, 1673–1693, https://doi.org/10.1175/1520-0469(2001)058<1673:CMTOTT>2.0.CO;2.

Chen, F., and J. Dudhia, 2001: Coupling an advanced land surface-hydrology model with the Penn State–NCAR MM5 modeling system. Part I: Model implementation and sensitivity. *Mon. Wea. Rev.*, **129**, 569–585, https://doi.org/10.1175/1520-0493(2001)129<0569:CAALSH>2.0.CO;2.

——, S. Miao, M. Tewari, J. W. Bao, and H. Kusaka, 2011: A numerical study of interaction between surface forcing and sea breeze circulation and their effects on stagnation in the greater Houston area. *J. Geophys. Res.*, **116**, D12105, https://doi.org/10.1029/2010JD015533.

Cheng, F. Y., and D. W. Byun, 2008: Application of high-resolution land use and land cover data for atmospheric modeling in the Houston–Galveston metropolitan area, Part I: Meteorological simulation results. *Atmos. Environ.*, **42**, 7795–7811, https://doi.org/10.1016/j.atmosenv.2008.04.055.

Cohen, A. E., S. M. Cavallo, S. M. Michael, C. Coniglio, and H. E. Brooks, 2015: A review of planetary boundary layer parameterization schemes and their sensitivity in simulating southeastern U.S. cold season severe weather environments. *Wea. Forecasting*, **30**, 591–612, https://doi.org/10.1175/WAF-D-14-00105.1.

Coniglio, M., C. J. Correia, P. T. Marsh, and F. Kong, 2013: Verification of convection-allowing WRF model forecasts of the planetary boundary layer using sounding observations. *Wea. Forecasting*, **28**, 842–862, https://doi.org/10.1175/WAF-D-12-00103.1.

Dee, D. P., and Coauthors, 2011: The ERA-Interim reanalysis: Configuration and performance of the data assimilation system. *Quart. J. Roy. Meteor. Soc.*, **137**, 553–597, https://doi.org/10.1002/qj.828.

Dirks, R. A., 1974: Urban atmosphere: Warm dry envelope over St. Louis. *J. Geophys. Res.*, **79**, 3473–3475, https://doi.org/10.1029/JC079i024p03473.

Dudhia, J., 1989: Numerical study of convection observed during the Winter Monsoon Experiment using a mesoscale two-dimensional model. *J. Atmos. Sci.*, **46**, 3077–3107,

https://doi.org/10.1175/1520-0469(1989)046<3077:NSOCOD>2.0.CO;2.

Dupont, S., T. L. Otte, and J. K. S. Ching, 2004: Simulation of meteorological fields within and above urban and rural canopies with a mesoscale model (MM5). *Bound.-Layer Meteor.*, **113**, 111–158, https://doi.org/10.1023/B:BOUN.0000037327.19159.ac.

Fan, H., and D. J. Sailor, 2005: Modeling the impacts of anthropogenic heating on the urban climate of Philadelphia: A comparison of implementations in two PBL schemes. *Atmos. Environ.*, **39**, 73–84, https://doi.org/10.1016/j.atmosenv.2004.09.031.

García-Díez, M., J. Fernández, L. Fita, and C. Yagüe, 2013: Seasonal dependence of WRF model biases and sensitivity to PBL schemes over Europe. *Quart. J. Roy. Meteor. Soc.*, **139**, 501–514, https://doi.org/10.1002/qj.1976.

Gunwani, P., and M. Mohan, 2017: Sensitivity of WRF model estimates to various PBL parameterizations in different climatic zones over India. *Atmos. Res.*, **194**, 43–65, https://doi.org/10.1016/j.atmosres.2017.04.026.

Haeger-Eugensson, M., and B. Holmer, 1999: Advection caused by the urban heat island circulation as a regulating factor on the nocturnal urban heat island. *Int. J. Climatol.*, **19**, 975–988, https://doi.org/10.1002/(SICI)1097-0088(199907)19:9<975::AID-JOC399>3.0.CO;2-J.

Heaviside, C., X. M. Cai, and S. Vardoulakis, 2015: The effects of horizontal advection on the urban heat island in Birmingham and the West Midlands, United Kingdom during a heatwave. *Quart. J. Roy. Meteor. Soc.*, **141**, 1429–1441, https://doi.org/10.1002/qj.2452.

Hong, S.-Y., J. Dudhia, and S.-H. Chen, 2004: A revised approach to ice microphysical processes for the bulk parameterization of clouds and precipitation. *Mon. Wea. Rev.*, **132**, 103–120, https://doi.org/10.1175/1520-0493(2004)132<0103:ARATIM>2.0.CO;2.

——, Y. Noh, and J. Dudhia, 2006: A new vertical diffusion package with an explicit treatment of entrainment processes. *Mon. Wea. Rev.*, **134**, 2318–2341, https://doi.org/10.1175/MWR3199.1.

Hu, X.-M., J. W. Nielsen-Gammon, and F. Zhang, 2010: Evaluation of three planetary boundary layer schemes in the WRF model. *J. Appl. Meteor. Climatol.*, **49**, 1831–1844, https://doi.org/10.1175/2010JAMC2432.1.

——, P. Klein, and M. Xue, 2013: Evaluation of the updated YSU planetary boundary layer scheme within WRF for wind resource and air quality assessments. *J. Geophys. Res. Atmos.*, **118**, 10 490–10 505, https://doi.org/10.1002/jgrd.50823.

Huang, M., Z. Q. Gao, S. G. Miao, and F. Chen, 2019: Sensitivity of urban boundary layer simulation to urban canopy models and PBL schemes in Beijing. *Meteor. Atmos. Phys.*, **131**, 1235–1248, https://doi.org/10.1007/s00703-018-0634-1.

Janjić, Z. I., 1994: A step-mountain eta coordinate model: Further developments of the convection, viscous sublayer, and turbulence closure schemes. *Mon. Wea. Rev.*, **122**, 927–945, https://doi.org/10.1175/1520-0493(1994)122<0927:TSMECM>2.0.CO;2.

Jiménez, P. A., J. Dudhia, J. F. González-Rouco, J. P. Montávez, E. García-Bustamante, J. Navarro, J. Vilà-Guerau De Arellano, and A. Muñoz-Roldán, 2013: An evaluation of WRF's ability to reproduce the surface wind over complex terrain based on typical circulation patterns. *J. Geophys. Res. Atmos.*, **118**, 7651–7669, https://doi.org/10.1002/jgrd.50585.

Kain, J. S., 2004: The Kain–Fritsch convective parameterizations: An update. *J. Appl. Meteor.*, **43**, 170–181, https://doi.org/10.1175/1520-0450(2004)043<0170:TKCPAU>2.0.CO;2.

Kolling, J. S., J. E. Pleim, H. E. Jeffries, and W. Vizuete, 2012: A multisensor evaluation of the asymmetric convective model, version 2, in southeast Texas. *J. Air Waste Manage.*, **63**, 41–53, https://doi.org/10.1080/10962247.2012.732019.

Kusaka, H., and F. Kimura, 2004: Coupling a single-layer urban canopy model with a simple atmospheric model: Impact on urban heat island simulation for an idealized case. *J. Meteor. Soc. Japan*, **82**, 67–80, https://doi.org/10.2151/jmsj.82.67.

——, H. Kondo, Y. Kikegawa, and F. Kimura, 2001: A simple single-layer urban canopy model for atmospheric models: Comparison with multilayer and slab models. *Bound.-Layer Meteor.*, **101**, 329–358, https://doi.org/10.1023/A:1019207923078.

Lamraoui, F., J. F. Booth, C. M. Naud, M. P. Jensen, and K. L. Johnson, 2019: The interaction between boundary layer and convection schemes in a WRF simulation of post cold frontal clouds over the ARM East North Atlantic site. *J. Geophys. Res. Atmos.*, **124**, 4699–4721, https://doi.org/10.1029/2018JD029370.

Lee, S. H., and Coauthors, 2011: Evaluation of urban surface parameterizations in the WRF model using measurements during the Texas Air Quality Study 2006 field campaign. *Atmos. Chem. Phys.*, **11**, 2127–2143, https://doi.org/10.5194/acp-11-2127-2011.

Lemonsu, A., and V. Masson, 2002: Simulation of a summer urban breeze over Paris. *Bound.-Layer Meteor.*, **104**, 463–490, https://doi.org/10.1023/A:1016509614936.

Lin, J.-L., M. Zhang, and B. Mapes, 2005: Zonal momentum budget of the Madden–Julian oscillation: The source and strength of equivalent linear damping. *J. Atmos. Sci.*, **62**, 2172–2188, https://doi.org/10.1175/JAS3471.1.

Liu, Y. B., F. Chen, T. Warner, and J. Basara, 2006: Verification of a mesoscale data-assimilation and forecasting system for the Oklahoma City area during the Joint Urban 2003 field project. *J. Appl. Meteor. Climatol.*, **45**, 912–929, https://doi.org/10.1175/JAM2383.1.

Lowry, W. P., 1977: Empirical estimation of urban effects on climate: A problem analysis. *J. Appl. Meteor.*, **16**, 129–135, https://doi.org/10.1175/1520-0450(1977)016<0129:EEOUEO>2.0.CO;2.

Mittal, R., M. Tewari, C. Radhakrishnan, P. Ray, T. Singh, and A. Nickerson, 2019: Response of tropical cyclone Phailin (2013) in the Bay of Bengal to climate perturbations. *Climate Dyn.*, **53**, 2013–2030, https://doi.org/10.1007/s00382-019-04761-w.

Mlawer, E. J., S. J. Taubman, P. D. Brown, M. J. Iacono, and S. A. Clough, 1997: Radiative transfer for inhomogeneous atmospheres: RRTM, a validated correlated-*k* model for the longwave. *J. Geophys. Res.*, **102**, 16 663–16 682, https://doi.org/10.1029/97JD00237.

Nakanishi, M., and H. Niino, 2006: An improved Mellor–Yamada level-3 model: Its numerical stability and application to a regional prediction of advection fog. *Bound.-Layer Meteor.*, **119**, 397–407, https://doi.org/10.1007/s10546-005-9030-8.

——, and ——, 2009: Development of an improved turbulence closure model for the atmospheric boundary layer. *J. Meteor. Soc. Japan*, **87**, 895–912, https://doi.org/10.2151/jmsj.87.895.

Nielsen-Gammon, J. W., 2002: Evaluation and comparison of preliminary meteorological modeling for the August 2000 Houston–Galveston ozone episode. Texas Natural Resource Conservation Commission Rep., 83 pp, https://oaktrust.library.tamu.edu/bitstream/handle/1969.1/158253/EvalComp_Preliminary_MM5_Modeling_2000Aug.pdf?sequence=1&isAllowed=y.

Oleson, K. W., G. B. Bonan, J. Feddema, M. Vertenstein, and C. S. B. Grimmond, 2008: An urban parameterization for a global climate model. Part I: Formulation and evaluation for two cities. *J. Appl. Meteor. Climatol.*, **47**, 1038–1060, https://doi.org/10.1175/2007JAMC1597.1.

Otte, T. L., A. Lacser, S. Dupont, and J. K. S. Ching, 2004: Implementation of an urban canopy parameterization in a mesoscale meteorological model. *J. Appl. Meteor.*, **43**, 1648–1665, https://doi.org/10.1175/JAM2164.1.

Ray, P., and C. Zhang, 2010: A case study of the mechanics of extratropical influence on the initiation of the Madden–Julian oscillation. *J. Atmos. Sci.*, **67**, 515–528, https://doi.org/10.1175/2009JAS3059.1.

——, ——, J. Dudhia, T. Li, and M. W. Moncrieff, 2012: Tropical channel model. *Climate Models*, L. M. Druyan, Ed., InTech, 3–18.

Salamanca, F., A. Martilli, M. Tewari, and F. Chen, 2011: A study of the urban boundary layer using different parameterizations and high-resolution urban canopy parameters with WRF. *J. Appl. Meteor. Climatol.*, **50**, 1107–1128, https://doi.org/10.1175/2010JAMC2538.1.

——, Y. Zhang, M. Barlage, F. Chen, A. Mahalov, and S. Miao, 2018: Evaluation of the WRF-Urban modeling system coupled to Noah and Noah-MP land surface models over a semiarid urban environment. *J. Geophys. Res. Atmos.*, **123**, 2387–2408, https://doi.org/10.1002/2018JD028377.

Sarmiento, D. P., K. J. Davis, A. Deng, T. Lauvaux, A. Brewer, and M. Hardesty, 2017: A comprehensive assessment of land surface-atmosphere interactions in a WRF/Urban modeling system for Indianapolis, IN. *Elementa Sci. Anthropocene*, **5**, 23, https://doi.org/10.1525/elementa.132.

Schwitalla, T., O. Branch, and V. Wulfmeyer, 2020: Sensitivity study of the planetary boundary layer and microphysical schemes to the initialization of convection over the Arabian Peninsula. *Quart. J. Roy. Meteor. Soc.*, **146**, 846–869, https://doi.org/10.1002/qj.3711.

Sharma, A., H. J. S. Fernando, A. F. Hamlet, J. J. Hellmann, M. Barlagee, and F. Chen, 2016: Urban meteorological modeling using WRF: A sensitivity study. *Int. J. Climatol.*, **37**, 1885–1900, https://doi.org/10.1002/joc.4819.

Shimada, S., T. Ohsawa, S. Chikaoka, and K. Kozai, 2011: Accuracy of the wind speed profile in the lower PBL as simulated by the WRF model. *SOLA*, **7**, 109–112, https://doi.org/10.2151/sola.2011-028.

Shin, H. H., and S.-Y. Hong, 2011: Intercomparison of planetary boundary-layer parameterizations in the WRF model for a single day from CASES-99. *Bound.-Layer Meteor.*, **139**, 261–281, https://doi.org/10.1007/s10546-010-9583-z.

Skamarock, W. C., and Coauthors, 2008: A description of the Advanced Research WRF version 3. NCAR Tech. Note NCAR/TN-475+STR, 113 pp., https://doi.org/10.5065/D68S4MVH.

Szymanowski, M., 2005: Interactions between thermal advection in frontal zones and the urban heat island of Wrocław, Poland. *Theor. Appl. Climatol.*, **82**, 207–224, https://doi.org/10.1007/s00704-005-0135-2.

Taha, H., 1999: Modifying a mesoscale meteorological model to better incorporate urban heat storage: A bulk-parameterization approach. *J. Appl. Meteor.*, **38**, 466–473, https://doi.org/10.1175/1520-0450(1999)038<0466:MAMMMT>2.0.CO;2.

——, 2008a: Urban surface modification as a potential ozone air-quality improvement strategy in California: A mesoscale modeling study. *Bound.-Layer Meteor.*, **127**, 219–239, https://doi.org/10.1007/s10546-007-9259-5.

——, 2008b: Meso-urban meteorological and photochemical modeling of heat island mitigation. *Atmos. Environ.*, **42**, 8795–8809, https://doi.org/10.1016/j.atmosenv.2008.06.036.

——, and R. Bornstein, 1999: Urbanization of meteorological models: Implications on simulated heat islands and air quality. *Int. Congress of Biometeorology and Int. Conf. on Urban Climatology*, Sydney, NSW, Australia, Macquarie University, http://www.met.sjsu.edu/faculty/bornstein.bak/urbanization/ICUC1_1_BOB-Taha.pdf.

Tan, H., P. Ray, M. Tewari, J. Brownlee, and R. S. Ajayamohan, 2019: Response of near-surface meteorological conditions to advection under the impact of green roof. *Atmosphere*, **10**, 759, https://doi.org/10.3390/atmos10120759.

Tewari, M., and Coauthors, 2004: Implementation and verification of the unified Noah land surface model in the WRF model. *20th Conf. on Weather Analysis and Forecasting/16th Conf. on Numerical Weather Prediction*, Seattle, WA, Amer. Meteor. Soc., 14.2a, https://ams.confex.com/ams/pdfpapers/69061.pdf.

Wang, J., J. Mao, Y. Zhang, T. Cheng, Q. Yu, J. Tan, and W. Ma, 2019: Simulating the effects of urban parameterizations on the passage of a cold front during a pollution episode in megacity Shanghai. *Atmosphere*, **10**, 79, https://doi.org/10.3390/atmos10020079.

Wong, K. K., and R. A. Dirks, 1978: Mesoscale perturbations on airflow in the urban mixing layer. *J. Appl. Meteor.*, **17**, 677–688, https://doi.org/10.1175/1520-0450(1978)017<0677:MPOAIT>2.0.CO;2.

Xie, B., J. C. H. Fung, A. Chan, and A. Lau, 2012: Evaluation of nonlocal and local planetary boundary layer schemes in the WRF model. *J. Geophys. Res.*, **117**, D12103, https://doi.org/10.1029/2011JD017080.

Yang, J., Z. H. Wang, F. Chen, S. Miao, M. Tewari, J. A. Voogt, and S. Myint, 2014: Enhancing hydrologic modelling in the coupled Weather Research and Forecasting–urban modelling system. *Bound.-Layer Meteor.*, **155**, 87–109, https://doi.org/10.1007/s10546-014-9991-6.

Zhang, D.-L., Y. X. Shou, R. R. Dickerson, and F. Chen, 2011: Impact of upstream urbanization on the urban heat island effects along the Washington–Baltimore corridor. *J. Appl. Meteor. Climatol.*, **50**, 2012–2029, https://doi.org/10.1175/JAMC-D-10-05008.1.